

# Chemical composition of stars with massive planets <sup>\*</sup>

T. Mishenina<sup>1</sup>, N. Basak<sup>1</sup>, V. Adibekyan<sup>2</sup>, C. Soubiran<sup>3</sup>, V. Kovtyukh<sup>1</sup>

<sup>1</sup>*Astronomical Observatory, Odessa National University, Shevchenko Park, 65014, Odessa, Ukraine,*

<sup>2</sup>*Instituto de Astrofísica e Ciências do Espaço, Universidade do Porto, CAUP, Rua das Estrelas, 4150-762 Porto, Portugal*

<sup>3</sup>*Laboratoire d'astrophysique de Bordeaux, Univ. Bordeaux, CNRS, B18N, allée Geoffroy Saint-Hilaire, 33615 Pessac, France*

Accepted, Received, in original form 23 April 2021

## ABSTRACT

Stellar parameters of 25 planet-hosting stars and abundances of Li, C, O, Na, Mg, Al, S, Si, Ca, Sc, Ti, V, Cr, Mn, Fe, Ni, Zn, Y, Zr, Ba, Ce, Pr, Nd, Sm and Eu, were studied based on homogeneous high resolution spectra and uniform techniques. The iron abundance [Fe/H] and key elements (Li, C, O, Mg, Si) indicative of the planet formation, as well as the dependencies of [El/Fe] on  $T_{cond}$ , were analyzed. The iron abundances determined in our sample stars with detected massive planets range within  $-0.3 < [\text{Fe}/\text{H}] < 0.4$ . The behaviour of [C/Fe], [O/Fe], [Mg/Fe] and [Si/Fe] relative to [Fe/H] is consistent with the Galactic Chemical Evolution trends. The mean values of C/O and [C/O] are  $\langle \text{C}/\text{O} \rangle = 0.48 \pm 0.07$  and  $\langle [\text{C}/\text{O}] \rangle = -0.07 \pm 0.07$ , which are slightly lower than solar ones. The Mg/Si ratios range from 0.83 to 0.95 for four stars in our sample and from 1.0 to 1.86 for the remaining 21 stars. Various slopes of [El/Fe] vs.  $T_{cond}$  were found. The dependencies of the planetary mass on metallicity, the lithium abundance, the C/O and Mg/Si ratios, and also on the [El/Fe]– $T_{cond}$  slopes were considered.

**Key words:** stars: abundances – stars: late-type – stars: planetary systems

## 1 INTRODUCTION

Over the past few decades, there has been an ongoing search for opportunities to study extrasolar planets based on characteristics of their hosting stars. The chemical composition features of parent stars considered as possible indicators of the presence of planetary systems, while elemental relationships can be essential for studying the formation of planets of different masses. Initially, the iron abundance [Fe/H] (Gonzalez 1997; Santos, Israelian & Mayor 2001; Udry & Santos 2007, and references therein), and the lithium abundance in stellar atmospheres (e.g. Gonzalez & Laws 2000; Gonzalez 2008; Israelian et al. 2004) came to the attention of researchers. Stars with massive Jupiter-like planets exhibited a [Fe/H] excess (e.g. Santos, Israelian & Mayor 2001; Fischer & Valenti 2005; Sousa et al. 2008), however such an excess was not obvious in stars hosting less massive planets, like Neptune- and Earth-sized ones (e.g. Udry & Santos 2007; Sousa et al. 2008); later, extrasolar planets were

also found around metal-deficient stars (Sousa et al. 2008; Adibekyan et al. 2012b,a). A detailed review with the results on the relationship between stellar metallicity and planet occurrence was recently presented by Adibekyan (2019).

As for lithium, in particular <sup>7</sup>Li, its lower abundance in stars with planetary systems, as compared to those without discovered planets, has been interpreted in favour of the presence of planets in these stars (e.g. Gonzalez & Laws 2000; Israelian et al. 2004; Gonzalez, Carlson & Tobin 2010; Israelian et al. 2009; Delgado Mena et al. 2015; Figueira et al. 2014; Mishenina et al. 2016). Meanwhile, an overabundance of the <sup>6</sup>Li isotope could suggest the presence of massive planets (e.g. Israelian et al. 2001; Montalbán & Rebolo 2002). For solar analogues (with  $T_{eff} \sim 5600\text{--}5900$  K), a significant difference in lithium abundance between stars with and without planets was detected by Delgado Mena et al. (2014); the authors noted that it was due not only to the differences in  $T_{eff}$ , [Fe/H] or age, but also to the possible presence of planets that caused additional rotationally-induced mixing in the external layers of planet-hosting stars. Yet, the observed lithium depletion, represented by a robust correlation between lithium abundance and the age of solar-like stars, (see, e.g. Baumann et al. 2010; Carlos, Nissen & Meléndez 2016),

\* Based on observations collected at OHP observatory, France

may reflect the evolution of the star rather than the presence of a planet.

Studying the CNO abundances in stars with and without planetary systems has not revealed any differences in the levels of these elements between the two groups of stars (e.g. Delgado Mena et al. 2010; da Silva, Milone & Reddy 2011; da Silva, Milone & Rocha-Pinto 2015; Nissen et al. 2014), while the elemental abundance trends with metallicities favored the Galactic chemical enrichment. Suárez-Andrés et al. (2016, 2017) demonstrated that the linear relationship between  $[N/Fe]$  and  $[Fe/H]$  was associated with the Galactic chemical evolution, as the planet-hosting stars tended to be richer in metals. They also found two different trends for  $[C/Fe]$  versus  $[Fe/H] > 0$  and  $[Fe/H] < 0$  and determined a flat distribution of the  $[C/Fe]$  ratio for all planetary masses.

The key role of carbon-to-oxygen (C/O) and magnesium-to-silicon (Mg/Si) ratios in planet-hosting stars, which can provide information about the protoplanetary discs wherein the respective planets are formed, has been revealed in, e.g., Kuchner & Seager (2005), Bond, O’Brien & Lauretta (2010). Theoretical calculations displayed that C/O and Mg/Si are the most important elemental ratios in determining the mineralogy of planets. The C/O ratio determines the distribution of Si among carbide and oxide species, while Mg/Si gives information about the silicate mineralogy (Bond, O’Brien & Lauretta 2010). However, currently available data on the abundances of these elements, in particular the C/O ratios, are quite contradictory and ambiguous, and there have been noticeable discrepancies in the estimates of the C and O abundances in various studies. For instance, Petigura & Marcy (2011) reported that planet-bearing systems were enriched in carbon with ratio  $\langle C/O \rangle = 1.00$ . Meanwhile, other studies have not confirmed that (e.g. Nissen 2013; Nissen et al. 2014) and shown that the stars with planets do not exhibit C/O ratios exceeding 0.8. According to Teske et al. (2014), the mean value of the C/O ratio in their sample of transiting exoplanet-host stars was 0.54, being equal to the solar value ( $C/O_{\odot} = 0.54$ ) and lower than the earlier measured  $\langle C/O \rangle$  value of about 0.65-0.75 in host stars. Pavlenko et al. (2019) reported that metal-rich dwarfs with planets were overabundant in carbon relative to Sun with an average difference  $\langle [C/O] \rangle = 0.05 \pm 0.05$ .

Adibekyan et al. (2015) found that the magnesium-to-silicon ratio  $[Mg/Si]$  in stars with low-mass planets was higher than in stars without planets. Despite the fact that the  $[Mg/Si]$  ratio depends significantly on metallicity through the Galactic chemical evolution, the difference in the  $[Mg/Si]$  ratio between low-mass planet hosts and non-hosts remains even after removing the Galactic evolution trend (Adibekyan et al. 2015). Adibekyan et al. (2017) took into account a plausible departure from Local Thermodynamic Equilibrium (NLTE) during the formation of the Mg lines and found out that the correction for the NLTE effects resulted in a small difference in  $[Mg/Si]$  ratios and that high  $[Mg/Si]$  values in the stars hosting super-Earth or Neptune-like planets were likely to be associated with their formation. The correlation between the C/O and Mg/Si ratios, that is critical for determining the mineralogy of planetary companions, has been studied in Suárez-Andrés et al. (2018). The authors obtained that 86% of stars among all stars with

high-mass companions have the carbon-to-oxygen ratio in the range of  $0.4 < C/O < 0.8$ , the remaining 14% having a C/O below 0.4; and the Mg/Si ratio is ranged within  $1 < Mg/Si < 2$  for all the stars with low-mass planets and for 85% of stars with high-mass companions (the other 15% have  $Mg/Si < 1$ ). Planet hosts with low-mass companions yielded C/O and Mg/Si ratios similar to the solar ones, whereas stars with high-mass companions exhibited lower C/O ratios. The existing contradictions in the data obtained inspire the need for new investigations of the abundances of elements to study the relationship of the abundances with the formation of planetary systems.

Udry & Santos (2007) pointed out that the relationship between volatile and refractory elements may be indicative of the presence of planets. Meléndez et al. (2009) showed that the Sun exhibited a depletion of refractory elements relative to volatiles as compared to the solar twins. Such a peculiarity could be related to the formation of planetary systems like our own, in particular to the existence of terrestrial planets (Meléndez et al. 2009). Moreover, later, it was shown that similar relationships could reflect a wide diversity of exoplanetary systems observed nowadays, as well as a variety of scenarios which could occur within the circumstellar discs (Spina, Meléndez & Ramírez 2016). Alternatively, it was also suggested that similar trends could also be associated with the correlation of elemental abundances with the age and place of birth in the Galaxy (e.g. González Hernández et al. 2013; Adibekyan et al. 2014, 2015; Nissen 2015), and hence not related to the presence of planets.

This paper aims to study the parameters and chemical composition of stars with detected massive planets in order to establish and verify the relationship between the presence of Jupiter-like planets and chemical composition of the respective parent stars. It provides an excellent opportunity to check how the peculiarities of the chemical composition of the planet host stars characterize the presence of planets and their properties, such as, masses. To this end, the lithium and the key elements for the formation of planetary systems (C, O, Mg, Si and their ratios), as well as the dependence of the contents of volatile and refractory elements on the condensation temperature  $T_{cond}$  will be considered as a function of planetary mass.

The paper is organized as follow. Observations and selection of stars are described in §2. The main stellar parameters are defined in §3. The abundance determinations and an error analysis are presented in §4. The analysis of the relationship between the presence of Jupiter-like planets and the chemical composition of the parent stars is reported in §5.

## 2 SAMPLE STARS AND OBSERVATIONS

A sample of planet-hosting stars with detected massive planets consisting of 24 stars with the planetary masses,  $M_{pl}$ , from 0.78 to 19.02  $M_J$  and one star with Neptun-size mass planet, that is 0.05  $M_J$  was selected from several papers related to a series of the SOPHIE Exoplanet Consortium programmes (Bouchy et al. 2009). We relied on the following sources: Boisse et al. (2012); Moutou et al. (2014); Courcol et al. (2015); Hébrard et al.

(2016); Díaz et al. (2016); Santos et al. (2016); Rey et al. (2017); Borgniet et al. (2019). The stellar and planetary characteristics of the sample planet hosts are presented in Table 1.

We used the stellar spectra from the OHP archive (Moultaka et al. 2004) obtained with the echelle spectrograph SOPHIE (Perruchot et al. 2011) at the resolving power  $R = 75,000$  restricted to the wavelength range  $4,400 - 6,800 \text{ \AA}$  and signal-to-noise ratio (S/N) higher than 80. The spectral processing, including normalisation of individual spectra to the local continuum, identification of spectral lines of different chemical elements, the line depth and equivalent width (EW) measurements, etc., was performed employing the spectrum with the highest S/N ratio for each star using the DECH30 software package developed by G.A. Galazutdinov <sup>1</sup>.

### 3 STELLAR PARAMETERS

The initial effective temperatures,  $T_{\text{eff}}$ , were derived through a method based on line-depth ratios for spectral-line pairs with different low-level excitation potentials taking advantage of the calibrations developed by Kovtyukh et al. (2003). Then, the final effective temperatures were determined by imposing the condition of independence of the Fe I abundance on the excitation potential. These latter temperatures are given in Table 1 and represent the values adopted for the abundance analysis.

The surface gravities  $\log g$  were obtained through the Fe I/Fe II ionisation balance, which means that the iron abundances derived from the lines of neutral and ionised iron were forced to be equal. In our case, the difference between these values does not exceed 0.03 dex. The microturbulent velocity  $V_t$  was determined by removing any correlation between the Fe I abundances and EWs of the lines. Using such iterative procedure, we determined the parameters by changing them sequentially, requiring that the slope of the Fe I abundances with respect to the excitation potential (for  $T_{\text{eff}}$ ) or EW (for  $V_t$ ) was almost zero and that the difference between the mean iron abundances obtained from the Fe I and Fe II lines did not exceed 0.03 dex (for  $\log g$ ). This procedure made it possible to determine  $T_{\text{eff}}$  with an accuracy ( $1 \sigma$ ) exceeding 60 K and both surface gravities and microturbulent velocity with an accuracy of about 0.1 dex. We employed the iron abundance obtained from the Fe I lines as the metallicity  $[\text{Fe}/\text{H}]$  of the studied stars. The neutral iron lines were used due to their large number in the spectra with known reliable atomic parameters.

A comparison of our parameter values with the data reported in the papers used for sampling the target stars is shown in Table 1. The difference between atmospheric parameters derived in this study and those earlier obtained by other authors (for all stars in common) is shown in Table 2. As results from the comparison of our  $T_{\text{eff}}$ ,  $\log g$ , and  $[\text{Fe}/\text{H}]$  with those determined by other authors, provided that the star HD 12484 is excluded (Petigura & Marcy 2011), the standard deviation of the difference does not exceed  $\pm 70 \text{ K}$ ,  $\pm 0.12$ , and  $\pm 0.10$ , respectively. The mean difference and

average standard deviation are  $1.6 \pm 49 \text{ K}$ ,  $-0.02 \pm 0.09$ , and  $-0.05 \pm 0.07$ , respectively. We also compared the parameter definitions reported by other authors for each investigated star. The differences between our parameter determinations and average values reported by other authors, but without measurements from the SOPHIE exoplanet consortium, are shown in Table 3 for each star of our sample. Such a comparison was made for 21 stars (as there were no parameter determinations reported by other authors for the remaining four stars). The differences and standard deviations resulting from the comparison of our data with the average values of  $T_{\text{eff}}$ ,  $\log g$ , and  $[\text{Fe}/\text{H}]$  reported by other authors are  $-9.9 \pm 38$ ,  $0.01 \pm 0.10$ ,  $0.06 \pm 0.06$ , respectively. The comparison of our data and those from literature is very good, as illustrated in Table 2 and Table 3.

### 4 CHEMICAL COMPOSITION

The elemental abundances were determined under the LTE condition employing the grid of model atmospheres (Castelli & Kurucz 2004). The each stellar model was obtained by interpolating on the grid in accordance with the required combination of stellar parameters  $T_{\text{eff}}$  and  $\log g$ . The Kurucz WIDTH9 code was used to determine the LTE abundance based the equivalent widths of lines of Na, Mg, Al, S, Si, Ca, Ti, Cr, Fe, Ni, Zn, Y, Zr, Ce, Pr, Nd and Sm elements. The list of used lines are presented in Table A1 in the Appendix (on line). We did not use strong lines (with EWs  $> 150 \text{ m\AA}$ ) due to noticeable effects of damping. The latest modified spectral synthesis code STARSP Tsymbal (1996) was employed to calculate the line profiles for Li, C, O, Sc, V, Mn, Ba, and Eu. The determination of the abundances of scandium, vanadium, manganese, barium and europium was carried out taking into account the hyperfine structure (HFS). We used five lines (5432.5, 6013.5, 6016.7, 6021.7, 6021.8  $\text{\AA}$ ) for manganese and two lines (4129.7 and 6645.1  $\text{\AA}$ ) for europium with and the HFS data from Prochaska & McWilliam (2000) and Ivans et al. (2006), respectively. For scandium, vanadium, and barium we took the parameters of HFS from the last version of VALD database <sup>2</sup>. We used five lines (5315.3, 5641.0, 5667.1, 5684.2, 6245.6  $\text{\AA}$ ) for scandium and four lines of vanadium (6081.4, 6090.2, 6242.8, 6243.1  $\text{\AA}$ ). For barium we explored three lines 5853.7, 6141.7, 6496.9  $\text{\AA}$ . The first two lines practically have an insignificant influence of the hyperfine structure; the 6496.9  $\text{\AA}$  line requires taking into account the HFS (Korotin et al. 2015). The damping constants for Ba lines are missing in VALD and we adopted the values from Korotin et al. (2015). All oscillator strengths were scaled by the solar isotopic ratios. Examples of some lines are shown in Fig. 1.

To compute synthetic spectra, the following effects were taken into consideration in addition to natural broadening of atomic lines: 1) instrumental broadening through the resolving power ( $R$ ) of the spectrograph; 2) the projection of the rotation velocity  $v \sin i$  obtained in the base papers and listed for each star in Table 1; and 3) large-scale atmospheric motions  $V_{\text{macro}}$ , determined by fitting the computed

<sup>1</sup> <http://www.gazinur.com/DECH-software.html>

<sup>2</sup> <http://vald.astro.uu.se/vald/php/vald.php>

**Table 1.** Stellar characteristics and planetary masses of the planet hosts sample.

Star	$T_{\text{eff}}$ (K)	$\log g$	[Fe/H]	Vt (km s <sup>-1</sup> )	$T_{\text{eff}}$ (K)	$\log g$	[Fe/H]	$v \sin i$ (km s <sup>-1</sup> )	$\log R'_{\text{HK}}$	planet	$M_{\text{pl}}$ ( $M_J$ )	ref
(our data)				(from literature)								
HD12484	5831	4.40	0.05	1.1	5920	4.65	0.05	8.2	-4.43	HD12484b	2.98	Hébrard et al. (2016)
HD13908	6150	4.00	0.05	1.0	6255	4.11	0.01	4.2	-4.90	HD13908b HD13908c	0.86 5.10	Moutou et al. (2014)
HD16175	5977	4.30	0.37	1.0	6022	4.21	0.37	5.1	-4.77	HD16175b	4.77	Díaz et al. (2016)
HD17674	5904	4.28	-0.15	0.8	5904	4.34	-0.16	2.3	-4.91	HD17674b	0.87	Rey et al. (2017)
HD24040	5800	4.25	0.23	0.8	-	-	-	-	-	HD24040b	4.0	Boisse et al. (2012)
HD29021	5550	4.30	-0.18	1.1	5560	4.44	-0.24	2.7	-5.00	HD29021b	2.4	Rey et al. (2017)
HD35759	5917	4.10	-0.04	0.9	6060	4.24	0.04	3.5	-5.36	HD35759b	3.76	Hébrard et al. (2016)
HD89307	5975	4.50	-0.05	0.7	-	-	-	-	-	HD89307b	2.0	Boisse et al. (2012)
HD113337	6750	4.30	0.14	1.3	6669	4.21	0.09	6.0	-	HD113337b	3.00	Borgniet et al. (2019)
HD141399	5515	4.35	0.47	0.7	5600	4.28	0.35	2.9	-5.26	HD141399b HD141399c HD141399d HD141399e	0.45 1.33 1.18 0.66	Hébrard et al. (2016)
HD143105	6280	4.30	0.01	1.7	6380	4.37	0.15	9.1	-5.00	HD143105b	1.21	Hébrard et al. (2016)
HD150706	5950	4.50	0.05	0.8	5961	4.50	-0.01	3.7	-4.47	HD150706b	2.71	Boisse et al. (2012)
HD154345	5503	4.40	-0.05	0.6	-	-	-	-	-	HD154345b	1.0	Boisse et al. (2012)
HD159243	6085	4.55	0.14	0.8	6123	4.55	0.05	3.8	-4.65	HD159243b HD159243c	1.13 1.9	Moutou et al. (2014)
HD164595	5725	4.40	-0.01	0.6	5790	4.44	-0.04	2.1	-4.86	HD164595b	0.05	Courcol et al. (2015)
HD191806	5807	4.30	0.36	0.7	6010	4.45	0.30	3.3	-4.85	HD191806b	8.52	Díaz et al. (2016)
HD214823	5980	3.90	0.13	1.2	6215	4.05	0.17	5.7	-4.79	HD191806c	19.4	Díaz et al. (2016)
HD219828	5850	4.10	0.18	1.0	5891	4.08	0.19	2.9	-5.12	HD219828b HD219828c	15.1 0.07	Santos et al. (2016)
HD220842	5938	4.15	-0.10	1.0	5960	4.24	-0.17	3.4	-5.17	HD220842b	3.18	Hébrard et al. (2016)
HD221585	5562	4.10	0.28	0.8	5620	4.05	0.29	3.7	-4.86	HD221585b	1.61	Díaz et al. (2016)
HD222155	5665	3.95	-0.05	0.6	5765	4.10	-0.11	3.2	-5.06	HD222155b	1.90	Boisse et al. (2012)
HIP65407	5354	4.50	0.35	0.5	5460	4.47	0.25	2.8	-4.60	HIP65407b HIP65407c	0.43 0.78	Hébrard et al. (2016)
HIP91258	5515	4.65	0.30	0.9	5519	4.53	0.23	3.5	-4.65	HIP91258b	1.07	Moutou et al. (2014)
HIP109384	5179	4.40	-0.24	0.8	5180	4.43	-0.26	2.7	-5.02	HIP109384b	1.56	Hébrard et al. (2016)
HIP109600	5525	4.65	-0.07	0.7	5530	4.45	-0.12	2.7	-5.07	HIP109600b	2.68	Hébrard et al. (2016)

**Table 2.** Mean difference and standard deviation between atmospheric parameters derived in this study and those obtained by other authors ( $n$  is the number of stars in common).

$\Delta T_{\text{eff}}$ , K	$\Delta \log g$	$\Delta [\text{Fe}/\text{H}]$	n	source
$-22 \pm 36$	$-0.02 \pm 0.12$	$-0.04 \pm 0.04$	9	Brewer et al. (2016)
$-10 \pm 28$	$-0.04 \pm 0.08$	$-0.02 \pm 0.10$	3	Takeda & Kawanomoto (2005), Takeda et al. (2007)
$25 \pm 35$	$0.04 \pm 0.06$	$-0.05 \pm 0.07$	7	Ramírez et al. (2012)
$10 \pm 84$	$-0.01 \pm 0.08$	$-0.05 \pm 0.12$	11	Petigura & Marcy (2011)
$-48 \pm 55$	$-0.11 \pm 0.12$	$-0.06 \pm 0.03$	6	Gonzalez, Carlson & Tobin (2010)
$29 \pm 44$	$0.05 \pm 0.08$	$-0.04 \pm 0.03$	7	Santos et al. (2013)
$38 \pm 64$	$0.00 \pm 0.08$	$-0.06 \pm 0.06$	7	Sousa et al. (2015)
$-9 \pm 44$	$-0.03 \pm 0.10$	$-0.08 \pm 0.07$	7	Aguilera-Gómez, Ramírez & Chanamé (2018)

synthetic spectrum from several unblended iron lines, factoring in  $v \sin i$ . Since for three stars, namely, HD 24040, HD 89307, and HD 154345 the  $v \sin i$  values in the basic works were missing, to calculate the synthetic spectrum, we have computed their rotational velocities ( $v \sin i$ ) using a relation, calibrated by Queloz et al. (1998) and giving  $v \sin i$  as a function of  $\sigma_{RV}$ , the standard deviation of the ELODIE cross-correlation function approximated by a Gaussian. We used the average  $\sigma_{RV}$  values from the ELODIE spectral archive of these stars. We obtained the following values: for HD 24040,

$v \sin i = 2.3 \text{ km s}^{-1}$ , for HD 89307,  $v \sin i = 2.6 \text{ km s}^{-1}$ , and for HD 154345,  $v \sin i = 1.3 \text{ km s}^{-1}$ . Gonzalez, Carlson & Tobin (2010) presented the  $v \sin i$  for two of these stars, namely, HD 89307,  $v \sin i = 2.9 \text{ km s}^{-1}$ , and HD 154345,  $v \sin i = 1.5 \text{ km s}^{-1}$ . All these values are consistent within the uncertainties and agree with those reported in Mishenina et al. (2012).

The determination of Li, C and O abundances based on the synthetic spectra calculations will be discussed in more detail below.

The use of the LTE approximation in our analysis does

**Table 3.** Comparison of stellar parameters obtained in this study and by other authors for some individual stars of our sample ("n" is the number of measurements of  $T_{\text{eff}}$ ,  $\log g$ , and  $[\text{Fe}/\text{H}]$ ).

HD/HIP	$T_{\text{eff}}$ , K	$\log g$ (our data)	$[\text{Fe}/\text{H}]$	$\langle T_{\text{eff}} \rangle$ , K	$\sigma$ , $\pm$	$\langle \log g \rangle$ (mean from literature)	$\sigma$ , $\pm$	$\langle [\text{Fe}/\text{H}] \rangle$	$\sigma$ , $\pm$	n	$\delta T_{\text{eff}}$ , K	$\delta \log g$	$\delta [\text{Fe}/\text{H}]$
12484	5831	4.40	0.05	5870	47	4.47	0.08	0.12	0.02	5,5,5	-39	-0.07	-0.07
13908	6150	4.00	0.05	6199	112	4.01	-	-0.08	-	3,1,1	-49	-0.01	0.13
16175	5977	4.30	0.37	5976	52	4.16	0.10	0.30	0.04	11,9,9	1	0.14	0.07
17674	5904	4.28	-0.15	5893	22	4.09	0.09	-0.18	0.05	8,4,5	11	0.19	0.03
24040	5800	4.25	0.23	5800	61	4.24	0.10	0.17	0.03	16,14,13	0	0.01	0.06
29021	5550	4.30	-0.18	5594	46	4.36	0.05	-0.22	0.07	5,3,3	-44	-0.06	0.04
35759	5917	4.10	-0.04	5998	-	-	-	-	-	1	-81	-	-
89307	5975	4.50	-0.05	5944	46	4.39	0.13	-0.15	0.05	16,15,14	31	0.11	0.10
113337	6750	4.30	0.14	6696	90	4.40	0.30	0.17	-	3,2,1	54	-0.10	-0.03
141399	5515	4.35	0.47	5570	44	4.21	0.04	0.34	0.02	2,2,2	-55	0.14	0.13
143105	6280	4.30	0.01	6262	42	-	-	-	-	2	18	-	-
150706	5950	4.50	0.05	5930	34	4.48	0.06	-0.04	0.04	15,13,13	20	0.02	0.09
154345	5503	4.40	-0.05	5458	61	4.44	0.11	-0.13	0.05	21,19,17	45	-0.04	0.08
159243	6085	4.55	0.14	6078	10	4.44	-	-	-	2,1,0	7	0.11	-
164595	5725	4.40	-0.01	5726	27	4.40	0.06	-0.08	0.03	18,16,16	-1	0.00	0.07
191806	5807	4.30	0.36	-	-	-	-	-	-	-	-	-	-
214823	5980	3.90	0.13	6008	148	3.90	0.04	0.09	0.07	4,2,2	-28	0.00	0.04
219828	5850	4.10	0.18	5856	52	4.13	0.06	0.15	0.03	14,13,12	-6	-0.03	0.03
220842	5938	4.15	-0.10	5909	50	4.19	0.03	-0.24	0.04	5,3,3	29	-0.04	0.14
221585	5562	4.10	0.28	5563	44	4.00	0.06	0.29	0.05	7,7,7	-1	0.10	-0.01
222155	5665	3.95	-0.05	5735	77	3.99	0.07	-0.16	0.05	9,8,7	-70	-0.04	0.11
HIP65407	5354	4.50	0.35	-	-	-	-	-	-	-	-	-	-
HIP91258	5515	4.65	0.30	-	-	-	-	-	-	-	-	-	-
HIP109384	5179	4.40	-0.24	5224	71	4.59	0.04	-0.28	0.07	2,2,2	-45	-0.19	0.04
HIP109600	5525	4.65	-0.07	-	-	-	-	-	-	-	-	-	-

not introduce significant inaccuracies into the obtained values of the abundances of elements, since the formation of the lines used in this work is not subject to a noticeable deviation from LTE in the considered range of stellar atmosphere parameters. Thus, the NLTE corrections depend on  $T_{\text{eff}}$  and  $\log g$ , but their values do not exceed 0.1 for the sodium lines 5688, 6154, 6160 Å (Korotin et al. 2014); 0.05 for magnesium lines of 4730, 5528, 5711, 6318, 6319.2, 6319.4 Å (Mishenina et al. 2004); 0.10-0.15 for aluminum 6696.0, 6698.6 Å lines (Andrievsky et al. 2008); 0.1 for barium 6141.71, 6496.90 Å lines, being insignificant for 5853.6 Å (Korotin et al. 2011), the strong barium line at 4554 Å was not included in our analysis; 0.05-0.10 for europium 4129.7 and 6645.1 Å lines (Mashonkina & Gehren 2000). An examination of possible NLTE effects on the manganese lines based on the abundance determinations from the lines of different multiplets (which have also been used in this study) does not show any systematic variations of abundances between these lines with the Mn abundances being correct within an uncertainty of 0.1 dex (Mishenina et al. 2015). Besides, as shown, for instance, by Adibekyan et al. (2017), the NLTE corrections to the Mg abundance determinations do not lead to any significant changes in the results or conclusions drawn earlier under LTE conditions.

The elemental abundances determined relative to the solar ones with the number of lines used for each element are listed in Table A2 in the Appendix (on line) for all target stars. The solar abundances were calculated by us earlier (Mishenina et al. 2017) using the solar EWs, which were measured from the reflected spectra of the Moon and asteroids obtained with the SOPHIE spectrograph. The oscillation

strengths,  $\log gf$ , of the lines are the same as the ones used in Mishenina et al. (2017) for the Sun, and are taken from the VALD (Kupka et al. 1999). A comparison of the adopted solar abundances with the solar elemental abundances reported by Asplund et al. (2009) was presented in Mishenina et al. (2017). In this study, we use the same list of lines as in Mishenina et al. (2017) and the solar abundance from Asplund et al. (2009).

#### 4.1 Li abundance

The Li abundances  $\log A(\text{Li})$  (in unit of  $\log A(\text{H}) = 12$ ) in the investigated stars were obtained by the  ${}^7\text{Li}$  line at 6707 Å through the spectral synthesis method. The line list around the Li I line is taken from Mishenina & Tsymbal (1997). An example of spectral fitting for the star HD 12484 is shown on the upper panel of Fig. 1. The study of departures from LTE in the case of the lithium line 6707 Å was presented in Lind, Asplund & Barklem (2009). For our target stars, the corrections do not exceed  $\pm 0.10$  dex.

Our Li abundances and their comparison with those obtained by the authors are given in Table 4. For HD 16175 and 113337, the Li abundances have not been determined due to the distortion of the spectrum in the region of the lithium line.

The results from different authors are in good agreement with the exception of stars exhibiting low lithium abundances. Such a discrepancy is mainly due to the difference in the quality of the employed spectra, resolving power (R), signal-to-noise ratio (S/N) and also to different stellar parameters.

**Table 4.** Our  $\log A(\text{Li})$  (column 1) compared with those obtained by other authors: 2 - Aguilera-Gómez, Ramírez & Chanamé (2018), 3 - Gonzalez, Carlson & Tobin (2010), 4 - Ramírez et al. (2012), 5 - Delgado Mena et al. (2015), 6 - Stonkutė et al. (2020).

HD	HIP	1	2	3	4	5	6
12484	9519	2.93	2.99	–	–	–	–
13908	10743	1.38	<1.35	–	–	–	–
16175	12191	–	2.68	2.45	–	2.78	–
17674	13291	1.8	–	–	–	–	–
24040	17960	1.1	0.99	–	–	–	–
29021	21571	1.0	–	–	–	–	–
35759	25883	2.73	–	–	–	–	–
89307	50473	2.25	2.23	2.1	–	2.31	–
113337	63584	–	–	–	–	–	–
141399	77301	0.7	–	–	–	–	–
143105	77838	2.3	–	–	–	–	–
150706	80902	2.6	2.59	2.46	–	–	2.55
154345	83389	<0.5	<-0.15	<-0.29	–	–	<0.05
159243	85911	2.6	–	–	–	–	–
164595	88194	1.0	0.78	–	0.75	–	<1.05
191806	99306	2.81	–	–	–	–	–
214823	111928	1.5	–	–	–	–	–
219828	115100	2.3	2.28	2.17	–	–	–
220842	115714	1.16	1.06	–	1.06	–	–
221585	116221	1.62	–	–	–	–	–
222155	116616	0.93	1.05	–	0.58	–	–
–	65407	1.09	–	–	–	–	–
–	91258	0.0	–	–	–	–	–
–	109384	0.5	0.34	–	0.34	–	–
–	109600	1.0	–	–	–	–	–

## 4.2 C and O abundances

The carbon abundances were determined in LTE approximations and using the following C I lines: 5052.17 Å ( $\log gf = -1.304$ ), 5380.34 Å ( $\log gf = -1.615$ ), 6587.61 Å ( $\log gf = -1.021$ ). Small NLTE corrections in the derived abundances lower than 0.05 dex were applied for the lines listed above (Caffau et al. 2010). A comparison between the synthetic and observed spectra for the CI lines at 5052 Å (HD 221585), and at 5380 Å line (HD 17674) is illustrated in Fig. 1 as an example.

The LTE abundances of oxygen were determined using the list of lines from the VALD database (Kupka et al. 1999, version 2018) by employing the [OI] line at 6300.30 Å ( $\log gf = -9.818$ ), which is unaffected by NLTE (Mishenina et al. 2000), taking into account the blending with Ni I line at 6300.34 Å, which is an isotopic splitting of  $^{58}\text{Ni}$  and  $^{60}\text{Ni}$ , with the total oscillator strength for the two isotopes  $\log gf = -2.11$  (Johansson et al. 2003). As an example, in Fig. 2 we present the resulting calculation of the oxygen line profile for four stars with different parameters. Our determinations of the C and O abundances and their comparison with the data reported by other authors are given in Table 5 and plotted in Fig. 3.

Our carbon abundances agree well with those obtained by Brewer et al. (2016); however, the data reported by Petigura & Marcy (2011), slightly differ from our values, which are lower.

## 4.3 Errors in abundance determinations

The statistical (internal) errors of abundance determinations were calculated as the quadratic sum of errors arising from the uncertainty of the atmospheric parameters. To estimate this we derived the elemental abundances for three stars with different parameters, namely, HD 113337 ( $T_{\text{eff}} = 6750$  K,  $\log g = 4.30$ ,  $Vt = 1.3$  km s $^{-1}$ ,  $[\text{Fe}/\text{H}] = 0.14$ ), HD 150706 ( $T_{\text{eff}} = 5950$  K,  $\log g = 4.50$ ,  $Vt = 0.8$  km s $^{-1}$ ,  $[\text{Fe}/\text{H}] = 0.05$ ), HIP 109384 ( $T_{\text{eff}} = 5179$  K,  $\log g = 4.40$ ,  $Vt = 0.8$  km s $^{-1}$ ,  $[\text{Fe}/\text{H}] = -0.24$ ) while changing  $T_{\text{eff}}$  of +70 K,  $\log g$  of +0.12, and  $Vt$  of = 0.10 km s $^{-1}$ . These values are somewhat different from the errors of the parameters indicated (stated) by us ( $\pm 60$  K,  $\pm 0.10$  dex,  $\pm 0.10$  km s $^{-1}$ ), but corroborated with the results of other authors obtained for individual stars and for the stars in common in different works and they may reflect systematic (external) errors that are typically due to use of different model atmospheres, codes, etc. The effects of uncertainties in atmospheric parameters on the accuracy of elemental abundance determinations for these stars is given in Table 6. As it can be seen from Table 6 the total abundance determination error for all elements does not exceed 0.10 dex. A comparison with the results of other authors has shown that external or systematic errors caused by different approaches and methods in the determination of stellar parameters, are comparable to our error values and should not significantly affect the results we obtained.

## 5 RESULTS AND DISCUSSION

The abundance of iron ( $[\text{Fe}/\text{H}]$ ) and lithium ( $\log A(\text{Li})$ ), as well as the carbon-to-oxygen (C/O) and magnesium-to-

**Table 5.** Our C and O abundance determinations compared with those obtained by other authors: 1 - Petigura & Marcy (2011), 2 - Brewer et al. (2016).

HD	HIP	[O/H] our	[C/H]	C/O	[O/H] 1	[C/H]	C/O	[O/H] 2	[C/H]	C/O
12484	9519	0.09	0.05	0.50	–	–0.15	–	0.09	0.05	0.50
13908	10743	0.01	–0.08	0.45	–	–	–	–	–	–
16175	12191	0.40	0.29	0.43	–	–	–	0.33	0.20	0.41
17674	13291	0.01	–0.11	0.48	–	–	–	–	–	–
24040	17960	0.14	0.13	0.54	0.15	0.18	0.59	0.20	0.14	0.48
29021	21571	–0.21	–0.18	0.59	–	–	–	–	–	–
35759	25883	0.16	0.04	0.42	–	–	–	–	–	–
89307	50473	0.08	–0.16	0.32	–	–	–	–	–	–
113337	63584	0.11	0.06	0.49	–	–	–	–	–	–
141399	77301	0.41	0.37	0.40	–	–	–	0.33	0.27	0.48
143105	77838	0.09	0.10	0.56	–	–	–	–	–	–
150706	80902	0.04	–0.10	0.40	–	–	–	–0.02	–0.01	0.56
154345	83389	–0.04	–0.15	0.43	–	–	–	–0.10	–0.15	0.49
159243	85911	0.06	0.04	0.53	–	–	–	–	–	–
164595	88194	–0.05	–0.07	0.53	–0.03	0.01	0.60	0.02	–0.05	0.47
191806	99306	0.28	0.25	0.51	–	–	–	–	–	–
214823	111928	0.11	0.05	0.48	0.02	0.10	0.66	0.25	0.04	0.34
219828	115100	0.13	0.11	0.53	–0.03	0.16	0.87	0.22	0.11	0.43
220842	115714	–0.06	–0.13	0.47	–	–	–	–	–	–
221585	116221	0.28	0.29	0.62	–	–	–	–	–	–
222155	116616	0.07	–0.11	0.36	–	–	–	–	–	–
–	65407	0.36	0.27	0.45	–	–	–	–	–	–
–	91258	0.31	0.27	0.48	–	–	–	–	–	–
–	109384	0.00	–0.13	0.41	–	–	–	–	–	–
–	109600	–0.06	–0.02	0.60	–	–	–	–	–	–

**Table 6.** Compilation of random errors due to uncertainties in atmospheric parameters. HD 113337 ( $T_{\text{eff}} = 6750$  K,  $\log g = 4.30$ ,  $Vt = 1.3$  km s $^{-1}$ ,  $[\text{Fe}/\text{H}] = 0.14$ ); HD 150706 (5950/4.50/0.8/ 0.05); HIP 109384 (5179/4.40/0.8/ –0.24).

El	HD 113337				HD 150706				HIP 109384			
	$\delta T_{\text{eff}+}$	$\delta \log g+$	$\delta Vt+$	tot+	$\delta T_{\text{eff}+}$	$\delta \log g+$	$\delta Vt+$	tot+	$\delta T_{\text{eff}+}$	$\delta \log g+$	$\delta Vt+$	tot+
Li I	0.05	0.01	0.01	0.05	0.06	–0.01	0.00	0.06	0.08	–0.01	0.00	0.08
C I	–0.02	0.03	0.00	0.04	–0.04	0.06	0.00	0.07	–0.06	0.03	0.00	0.07
O I	0.03	0.04	0.00	0.05	0.01	0.04	0.00	0.04	–0.02	0.05	0.00	0.05
Na I	0.03	–0.01	–0.01	0.03	0.03	–0.02	–0.01	0.04	0.05	–0.02	0.00	0.05
Mg I	0.02	0.01	–0.01	0.03	0.02	–0.01	–0.01	0.03	0.02	–0.02	0.00	0.03
Al I	0.03	0.00	0.00	0.03	0.04	–0.01	–0.01	0.05	0.03	–0.01	–0.01	0.03
Si I	0.02	0.00	–0.02	0.03	0.01	–0.01	–0.01	0.02	–0.01	–0.01	–0.01	0.02
S I	–0.01	–0.02	0.00	0.02	–0.04	0.05	0.00	0.06	–0.04	0.03	0.00	0.03
Ca I	0.05	–0.01	–0.02	0.05	0.04	–0.03	–0.02	0.05	0.06	–0.03	–0.02	0.07
Sc II	0.02	0.04	–0.01	0.05	0.00	0.05	–0.01	0.05	–0.01	0.04	–0.01	0.04
Ti I	0.05	0.01	0.00	0.05	0.05	–0.02	–0.01	0.05	0.08	–0.01	–0.02	0.08
Ti II	0.01	0.03	–0.01	0.03	0.00	0.05	–0.01	0.05	–0.01	0.05	–0.01	0.05
V I	0.05	0.00	0.00	0.05	0.07	–0.01	0.00	0.07	0.09	0.00	–0.01	0.09
Cr I	0.03	0.00	–0.01	0.03	0.04	–0.02	–0.01	0.05	0.06	0.00	0.00	0.06
Mn I	0.03	–0.01	–0.02	0.04	0.04	–0.02	–0.02	0.05	0.04	–0.02	–0.03	0.05
Fe I	0.04	0.00	–0.01	0.04	0.05	–0.01	–0.01	0.05	0.03	0.00	–0.01	0.03
Fe II	0.00	0.03	–0.02	0.04	–0.02	0.05	–0.01	0.05	–0.05	0.04	–0.01	0.06
Ni I	0.04	0.00	0.00	0.04	0.04	–0.01	0.00	0.04	0.01	0.02	–0.01	0.02
Zn I	0.04	0.01	–0.02	0.05	0.01	0.01	–0.02	0.03	–0.02	0.01	–0.02	0.03
Y II	0.02	0.04	0.00	0.04	0.00	0.04	0.00	0.04	0.00	0.05	0.00	0.05
Zr II	0.02	0.04	0.00	0.04	0.01	0.05	0.00	0.05	0.00	0.05	0.00	0.05
Ba II	0.05	0.01	–0.05	0.07	0.03	0.01	–0.04	0.05	0.02	0.01	–0.03	0.04
Ce II	0.03	0.04	0.00	0.05	0.01	0.04	0.00	0.04	0.00	0.04	–0.01	0.04
Pr II	0.04	0.04	0.00	0.06	0.01	0.04	0.00	0.04	0.00	0.04	–0.01	0.04
Nd II	0.03	0.04	0.00	0.05	0.02	0.05	0.00	0.05	0.01	0.05	–0.01	0.05
Sm II	0.02	0.04	0.00	0.04	0.01	0.04	–0.01	0.04	0.02	0.05	0.00	0.05
Eu II	0.03	0.04	0.00	0.05	0.00	0.04	0.00	0.04	–0.01	0.04	–0.01	0.04

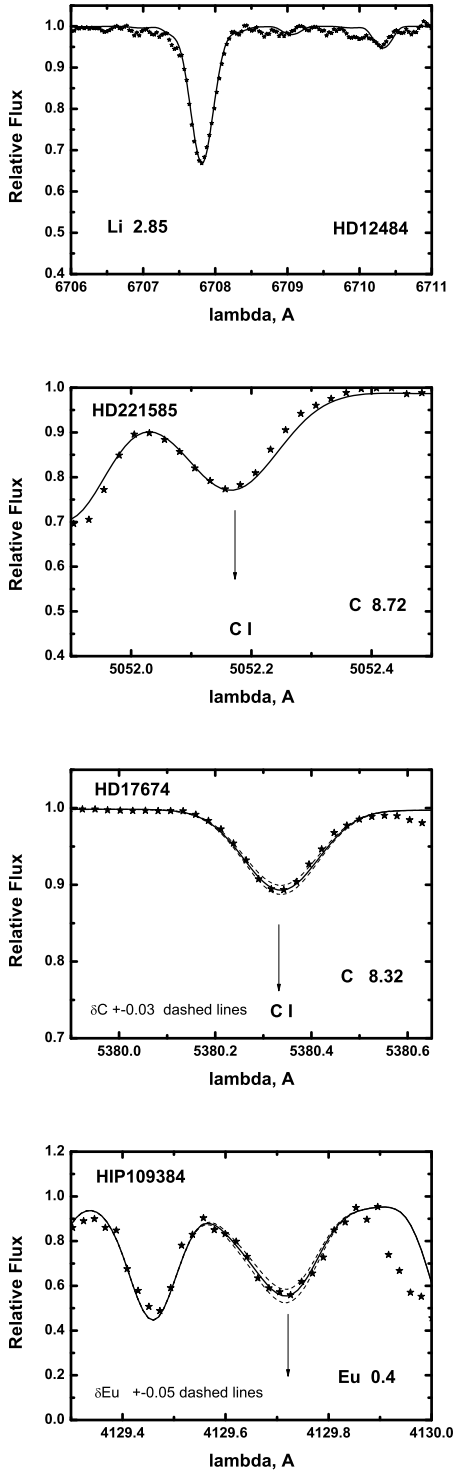


**Figure 1.** Observed (asterisks) and calculated (solid line) spectra in the region of Li I 6707 Å line for HD 12484 (top panel), CI 5052 Å line for HD 221585 and C I 5380 Å line for HD17674 (middle panels), Eu II 4129 Å line for HIP109384 (bottom panel).

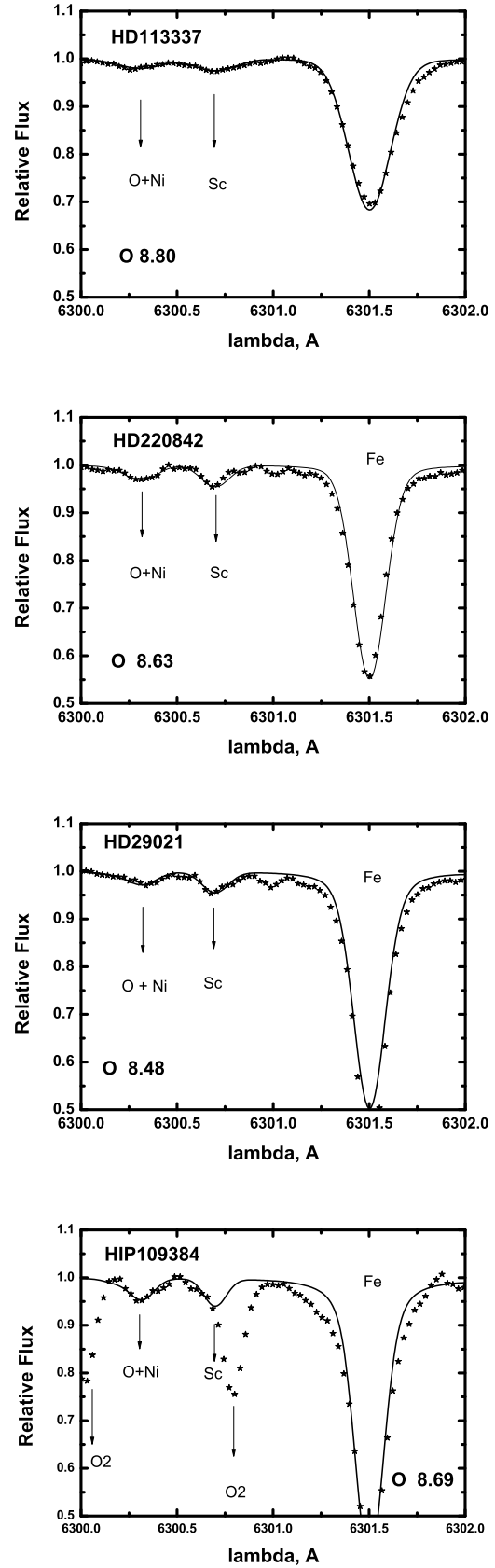


**Figure 2.** Observed (asterisks) and calculated (solid line) spectra in the region of [O I] 6300.3 Å line for four stars with different stellar parameters.



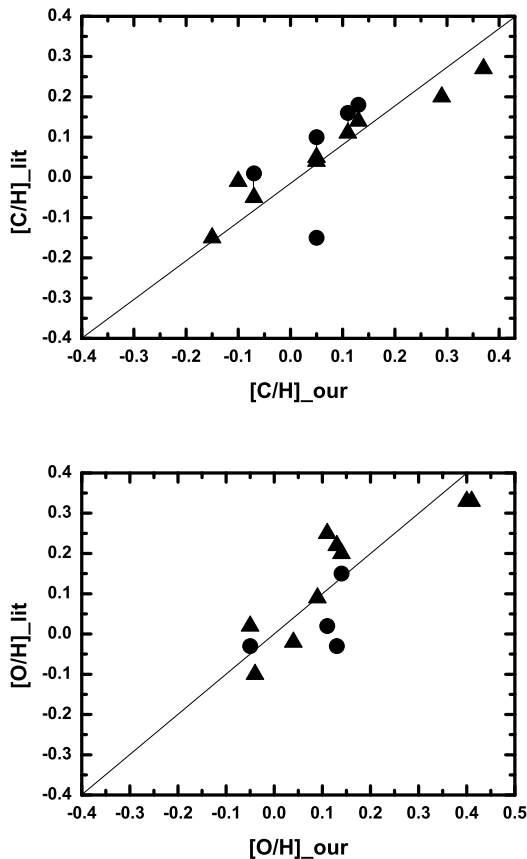


**Figure 3.** Our [C/H] and [O/H] values compared with those reported by Petigura & Marcy (2011) (circles) and Brewer et al. (2016) (triangles).

silicon (Mg/Si) ratios, are important parameters in studying planet host stars in depth. The ratio of volatiles to refractory elements may be an important key to understand the formation of low-mass terrestrial planets and giant-planet cores. A sample of stars with well-detected planetary systems, as that examined in this study, may clarify the possible constraints for the connection between these chemical parameters and the presence of planets. This is discussed in more detail below.

### 5.1 [Fe/H] versus $T_{\text{eff}}$

To explain the metallicity excess in massive exoplanet host stars, two hypotheses were proposed: the self-enrichment (or pollution) mechanism and a primordial origin of metal overabundance. The primordial cloud is the most likely origin for the metal richness of giant planet host stars (Gonzalez 1997). This hypothesis has been substantiated by models of planet formation and evolution, based on exoplanet formation scenarios as such the core accretion (CA) and tidal downsizing (see in detail, Adibekyan 2019, and references therein). The first statistics about extrasolar planets (Mortier et al. 2012) show that the presence of giant planets apparently depends on the stellar metallicity and mass. For instance, such planets are more frequently observed around metal-rich stars with an exponential increase in the planet occurrence rate

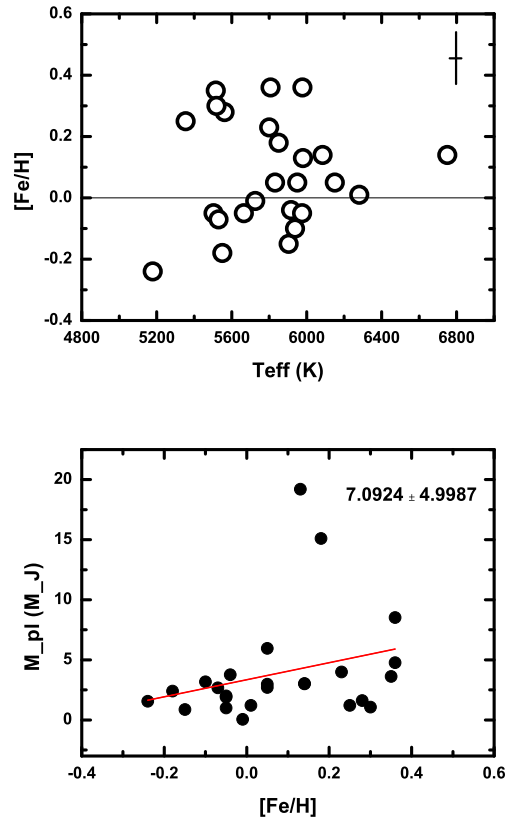


**Figure 4.** [Fe/H] versus  $T_{\text{eff}}$  and  $M_{\text{pl}}$  versus [Fe/H] for our target stars. The horizontal line corresponds to [Fe/H] = 0. The solid line in the lower panel represents a linear fit to the data with the value of the slope indicated in the plot.

with metallicity; the occurrence rate (or frequency) for hot Jupiters around metal-poor stars is less than 1.0% at one sigma and frequency is higher for star with [Fe/H]  $> -0.7$  than those with [Fe/H]  $< -0.7$  (Mortier et al. 2012).

The range of metallicities of the our sample is  $-0.3 < [\text{Fe}/\text{H}] < 0.4$ . The correlation between [Fe/H] and the effective temperature  $T_{\text{eff}}$  for our target stars is depicted in Fig. 4. As follows from the metallicity range of the studied stars massive planets in our sample are located not only around stars with metallicities higher than the solar one (in most cases), but also around stars with slight metal deficiencies. The bottom panel of Fig. 4 shows a positive correlation between planetary mass and metallicity. The trend seem to be present (slope of  $4.33 \pm 2.03$ ) even if the two most massive planets with masses greater than  $13 M_J$  (these objects can be Brown Dwarfs) are excluded. As discussed in Adibekyan (2019), there is a complex interdependence between planetary mass, stellar mass, and stellar metallicity, which makes difficult to identify the exact origin of the observed dependence of  $M_{\text{pl}}$  on [Fe/H].

### 5.2 Lithium abundance and exoplanets

The dependencies of the Li abundance on the stellar effective temperature  $T_{\text{eff}}$ , rotational velocity  $v \sin i$  and on age are plotted in Fig. 5. Evolutionary tracks for different ages of

Baraffe et al. (2017) and the Li abundance envelope in the Hyades (see top panel, Thorburn et al. 1993) are overplotted. Baraffe et al. (2017) studied lithium depletion in low-mass and solar-like stars as a function of time, applying a new diffusion coefficient describing extra-mixing occurring at the bottom of a convective envelope. We see that the lithium abundance behaviour reflects its depletion through stellar evolution.

The relationship between  $\log A(\text{Li})$  and rotational velocities  $v \sin i$  is depicted in the middle panel in Fig.5. The surface Li abundance of a star is highly sensitive to its rotational velocity during both main and pre-main sequence evolution (e.g. Beck et al. 2017; Bouvier et al. 2016). Beck et al. (2017) found that the measured  $A(\text{Li})$  were in good agreement with the  $A(\text{Li})$  evolution predicted from a grid of models, which included rotationally-induced internal mixing. The dependence obtained in this study reflects the role of rotation in the lithium abundance values, which could be associated with rotationally-induced internal mixing and also to some extent with stellar activity (see, e.g., Fig.5, panel  $v \sin i$  versus  $\log R'_{\text{HK}}$ ).

A very important aspect of studying the lithium content in solar analogues is related to the search for planetary systems and their occurrence. The correlation between the Li abundance and planet occurrence has been studied in a series of works, though there is still no clarity in this respect. For instance, as reported by Gonzalez & Laws (2000); Gonzalez (2008); Israelian et al. (2004, 2009); Delgado Mena et al. (2014); Figueira et al. (2014), planet-hosting stars are likely to have lower lithium abundances than stars without planetary systems. Meanwhile, Carlos, Nissen & Meléndez (2016) have discovered that the lithium abundance in solar-twin stars depends on stellar age while there was no indication of any relationship between planet-hosting stars and strong lithium depletion. Our determination of the Li abundance versus age is shown in Fig.5 (bottom panel), using the age data from baseline papers. The plot shows a negative trend at about  $1\text{-}\sigma$  significance level. Despite our sample has a wider  $T_{\text{eff}}$  range than solar twins, there seems to be a trend of Li versus age. Given the presence of complex relationships between lithium content, rotational velocities  $v \sin i$ , stellar activity and the influence of magnetic fields (see, e.g. Mishenina et al. 2012; Katsova, Livshits & Mishenina 2013), it appears that this dependence reflects the role of various physical processes that affect the lithium abundance rather than results from the presence of planetary systems.

The relationship between the Li abundance and planetary mass can be seen in Fig.6. The absence of a large number of stars hosting planets with masses exceeding  $5 M_J$  in our sample does not allow us to draw reliable conclusions.

### 5.3 C and O in exoplanet host stars

The obtained values of  $[\text{C}/\text{H}]$ ,  $[\text{C}/\text{Fe}]$ ,  $[\text{O}/\text{H}]$ ,  $[\text{O}/\text{Fe}]$  vs.  $[\text{Fe}/\text{H}]$  are shown in Fig. 7. The C/O,  $[\text{C}/\text{O}]$  vs.  $[\text{Fe}/\text{H}]$  and C/O,  $[\text{C}/\text{Fe}]$  vs. planetary masses  $M_{pl}$  are depicted in Fig. 8. As can be seen in Fig. 7, the trends of  $[\text{C}/\text{H}]$  and  $[\text{O}/\text{H}]$  vs.  $[\text{Fe}/\text{H}]$  are corroborated by the data obtained earlier (see Delgado Mena et al. 2010, their Figs.1,3), and (Suárez-Andrés et al. 2017, their Fig.5). The obtained

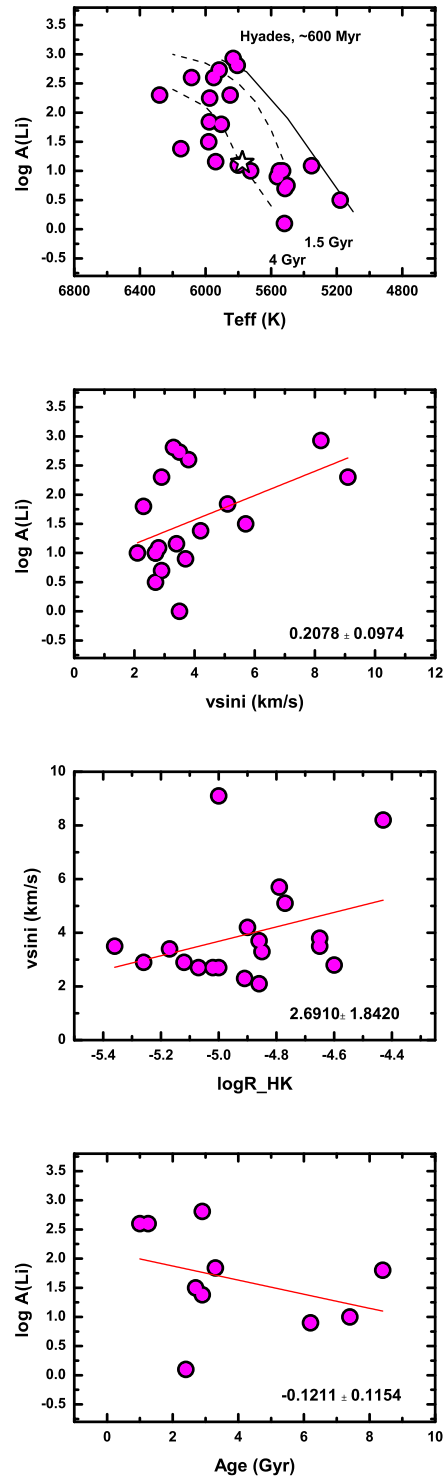


**Figure 5.** Dependences of the Li abundance on stellar effective temperature ( $T_{\text{eff}}$ ) and rotational velocity ( $v \sin i$ ) and stellar age for our target stars. Dependence of  $v \sin i$  on chromospheric activity  $\log R'_{\text{HK}}$  (third panel from the top). In the top panel, also plotted are the evolutionary tracks from Baraffe et al. (2017) for different ages (dashed lines) and the Li abundance envelope in the Hyades from Thorburn et al. (1993) (solid line). Position of the Sun is marked with an asterisk, the solar parameters are taken from Jofré et al. (2015).

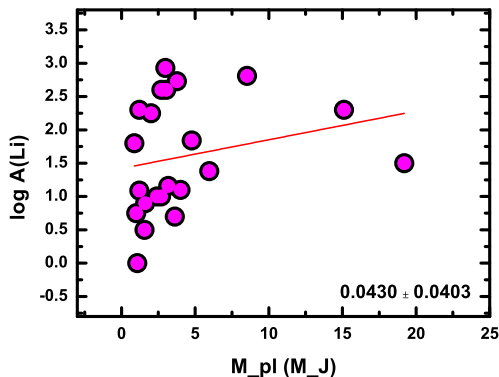


**Figure 6.** Dependences of the Li abundance on planetary mass  $M_{pl}$  for our target stars.

dependence of  $[C/H]$ ,  $[O/H]$  on the metallicity  $[Fe/H]$  reflects the well-known fact that the production of carbon and oxygen in the Galaxy (in absolute terms) rises with an increase of the metallicity due to an additional contribution to the enrichment, besides massive collapsing supernovae (CCSN or SN II Type), in which oxygen is the dominant element ejected (Woosley & Weaver 1995), massive fast-rotating stars, (Maeder & Meynet 2012), also from SN Ia and Asymptotic Giant Branch (AGB) stars, whose yields of elements grow with increasing metallicity above  $[Fe/H] = -1.0$  (e.g. Timmes, Woosley & Weaver 1995; Nomoto, Thielemann & Yokoi 1984; Käppeler et al. 2011; Prantzos et al. 2018).

Decreasing  $[C/Fe]$  and  $[O/Fe]$  ratios with increasing stellar metallicity (Fig.7) corroborate observations of C and O in the Galactic disc (e.g. Delgado Mena et al. 2010; Petigura & Marcy 2011; Nissen et al. 2014; Suárez-Andrés et al. 2017). According to models of Galactic Chemical Evolution (GCE), Type Ia supernovae start ejecting large amounts of iron and negligible amounts of oxygen into the interstellar medium beyond about 1 Gyr, which causes the distinct downturn of  $[O/Fe]$  to the solar value. Suárez-Andrés et al. (2017) drew attention to two differing patterns of behaviour of carbon at  $[Fe/H]$  below and above solar value (see their Figure 5). It may be associated, first of all, with different nucleosynthesis (sources) of carbon and oxygen at such metallicities, but not with the fact that stars with massive planets richer in metals exhibit differing C and O abundances. Reaching more reliable conclusions require the use of a larger sample of stars and involve the study of the GCE, which is beyond the scope of this paper. Moreover, Suárez-Andrés et al. (2017) did not find any clear relationship between the  $[C/Fe]$  abundance ratio and planetary mass. Fig. 8 (bottom panel) substantiates such a result. Therefore, the C and O abundances in our target stars demonstrate that the behaviour of carbon and oxygen in stars with planetary systems in the Galactic disc is quite typical of stars inhabiting the thin disc.

The carbon-to-oxygen ratio C/O is one of the important characteristics of the structure and chemical composition of planets. Theoretical models of planet formation and evolution consider both refractory (Bond, O’Brien & Lauretta

2010) and volatile elements (Thiabaud et al. 2015a), which can provide information about the protoplanetary disc in which the planet was formed. Models by Thiabaud et al. (2015b) show that condensation of volatiles varies with the radial distance and that the C/O ratio can be four times the solar value in certain regions of the protoplanetary disc. This may lead to the formation of planets with C/O values in their shells being more than three times the solar value.

Over several years of investigation of the chemical composition, the values of this ratio for planet hosts and non-hosts obtained in different studies have varied from  $C/O \geq 1$  (e.g. Petigura & Marcy 2011) to near solar value ( $C/O_{\odot} = 0.54$ ) (Teske et al. 2014). The differences in the obtained C abundances may be associated with a number of factors, primarily the use of various markers of the carbon abundance (atomic and molecular lines), atomic and molecular parameters (e.g.  $\log g_f$ ), quality of spectra, application of different model atmospheres and methods, and samples of stars, etc. In this regard, it is important to determine reliable C and O abundances and seek for correlations between the abundances of these elements and properties of planets.

The mean value of  $\langle C/O \rangle$  for our target is  $\langle C/O \rangle = 0.48 \pm 0.07$ , which agrees well with the mean value of  $\langle C/O \rangle = 0.45 \pm 0.06$  obtained by Brewer et al. (2016), normalized to the solar carbon abundance adopted in their study (Grevesse, Asplund & Sauval 2007) for nine stars in common. At the same time, the mean C/O ratio is slightly different from the mean  $C/O = 0.68 \pm 0.13$  obtained by Petigura & Marcy (2011) for four stars in common. There is only one star in our sample in common with the study by Stonkutė et al. (2020), namely HD 150706, for which the C, O abundances, as well as the C/O ratio, are reported; these values show good agreement.

As mentioned earlier, Delgado Mena et al. (2010) and Petigura & Marcy (2011) found that a significant percentage of high-metallicity solar-type stars have  $C/O > 0.8$ ; however, it has been demonstrated in a number of later works that not so many stars actually have C/O greater than 0.8 (Nissen 2013; Brewer et al. 2016; Suárez-Andrés et al. 2018; Stonkutė et al. 2020). Nissen et al. (2020) have indicated that their 3D non-LTE C/O values support a rising trend with decreasing age for the old (red) sequence, though all the stars have C/O ratios clearly below 0.8. All nine stars with  $C/O = 0.7$  have been confirmed to host planets and they all exhibit high metallicities ranging within  $0.18 < [Fe/H] < 0.31$ . The authors have concluded that it is not feasible to deduce from their small sample of stars whether it is a high C/O ratio or a high  $[Fe/H]$  (or both) that favours the formation of planets.

The C/O ratios obtained in this study range from 0.32 to 0.62 with the mean value of  $\langle C/O \rangle = 0.48 \pm 0.07$ , which is well consistent with the data of Suárez-Andrés et al. (2018). The stars with massive planets investigated in this study show a wide range of C/O ratios, but do not exhibit such a high C/O ratio close to 0.8. In this study, the mean value relative to the solar one is  $\langle [C/O] \rangle = -0.07 \pm 0.07$ ; it enables us to deduce that our studied stars with massive planets have  $[C/O]$  ratios slightly lower, but close to the solar one within the errors. This result does not unambiguously confirm the finding reported by Pavlenko et al. (2019), in particular that the metal-rich dwarfs with planets are overabundant in carbon with an average difference of

$\langle [C/O] \rangle = 0.05 \pm 0.05$ ; in our case for stars with  $[Fe/H] > 0$  this value is  $\langle [C/O] \rangle = -0.05 \pm 0.05$ . In Fig.8, the C/O ratio is also shown as a function of the planetary mass, but no trend is evident.

#### 5.4 Mg and Si in planet host stars

Magnesium and silicon are key planet-building elements and Mg/Si ratio may be used to detect low-mass planets and specify their chemical composition and mineralogy (Bond, O'Brien & Laretta 2010). Thiabaud et al. (2015b) have shown that the elemental ratios Mg/Si and Fe/Si in planets are essentially identical to those in the star. Our result for Mg and Si are listed in Table A2 in Appendix and their comparison with the values for the main sequence stars reported in Mishenina et al. (2016) is depicted in Fig. 9 (upper panel). The stars studied in Mishenina et al. (2016) have the same range of parameters as the stars of the current work and belong to the Galactic thin disc.

As can be seen from Fig.9, the dependence of Mg/Fe on  $[Fe/H]$  is similar to the trend for dwarfs that substantiates the findings in Adibekyan et al. (2015), in particular, that the  $[Mg/Si]$  ratio depends significantly on metallicity through the GCE. Later, Brewer et al. (2016) also showed that the Mg and Si behaviour could reflect the overall metallicity trend traced by  $[Fe/H]$ , i.e. the GCE.

We obtained Mg/Si ratios ranging from 0.83 to 0.96 for four stars of our sample with high-mass planets and from 1.0 to 1.8 for the remaining 21 stars. It supports the finding in Suárez-Andrés et al. (2018), that 85% stars with high-mass companions have the Mg/Si ratios between one and two while the other 15% exhibit Mg/Si values below one.

Fig.9 (bottom panel) illustrates the dependence of  $[Mg/Si]$  on planetary masses. Just a trace of a downward trend can be seen in this figure; however, the large scatter of the  $[Mg/Si]$  values in the region of lower masses (1-5  $M_J$ ), along with the small number of stars with planets of masses exceeding 10  $M_J$ , do not allow us to draw a confident conclusion about the dependence of the planetary mass on the  $[Mg/Si]$  ratio in the host star.

## 6 ELEMENTAL ABUNDANCES VERSUS CONDENSATION TEMPERATURES $T_{COND}$

As reported in Udry & Santos (2007), the stars known to host giant planets are expected to be more enriched in refractory elements (i.e. elements with high condensation temperature  $T_{cond}$ ), because volatiles (having low  $T_{cond}$ ) may evaporate from infalling bodies before being accreted (e.g. Gonzalez 1998; Smith, Cunha & Lazzaro 2001; Ecuillon et al. 2006). As noted earlier by Guillot (2005), the cores of Jupiter, Saturn, Uranus and Neptune may contain heavy metals in the form of rocks and ices, which means that these (massive) planets possess dense cores of different masses. Based on a correlation between the difference of abundance in the Sun and mean values in non-hosts with condensation temperature  $T_{cond}$ , Meléndez et al. (2009) found that volatile elements are more abundant in the Sun relative to the solar twins while elements that easily form dust, i.e., refractories, are underabundant. González Hernández et al. (2013) obtained clear up-

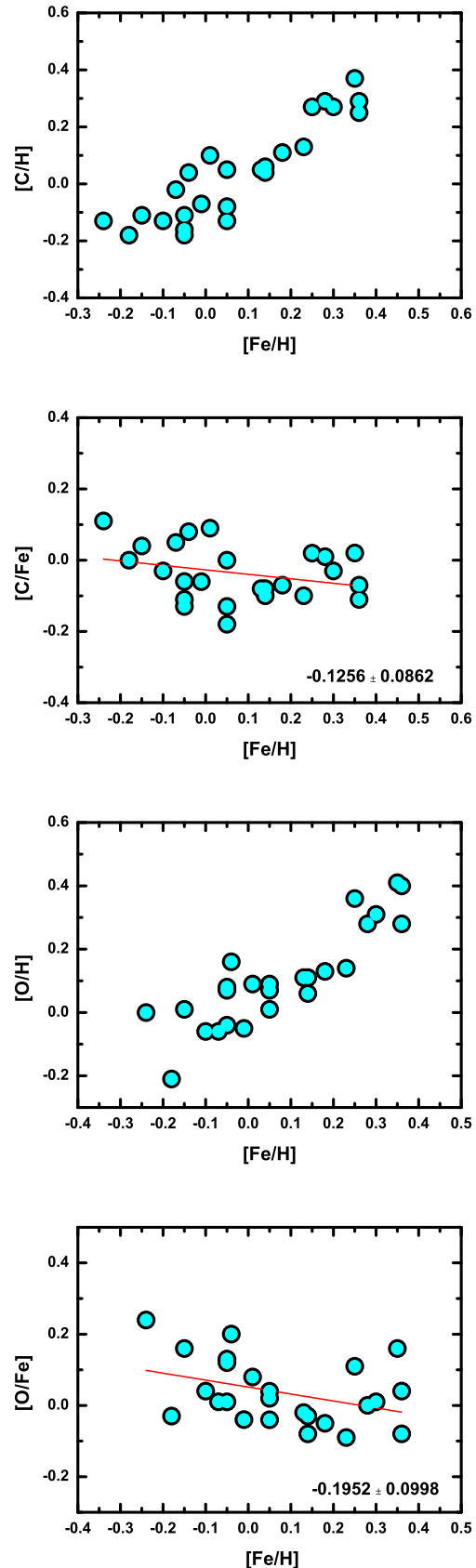
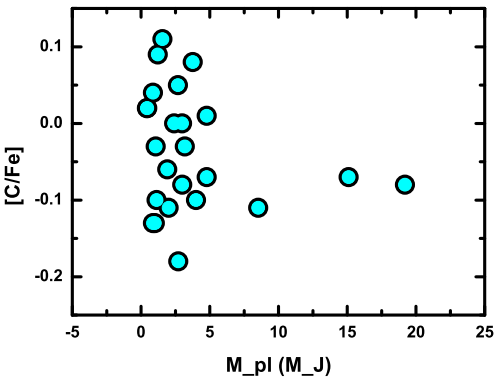
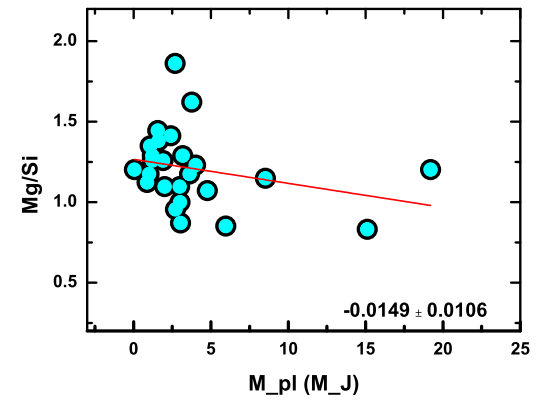
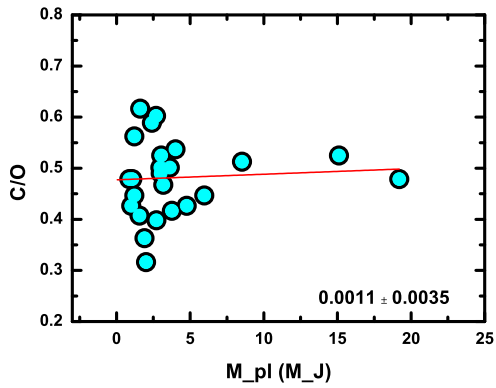
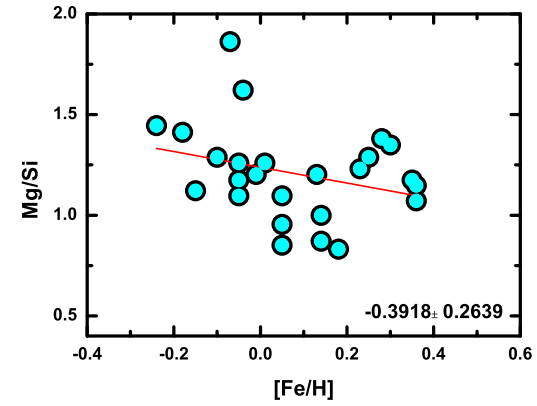
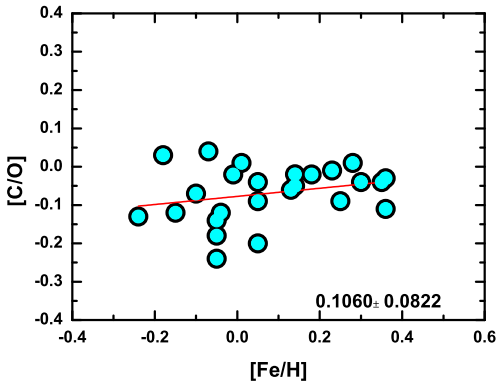
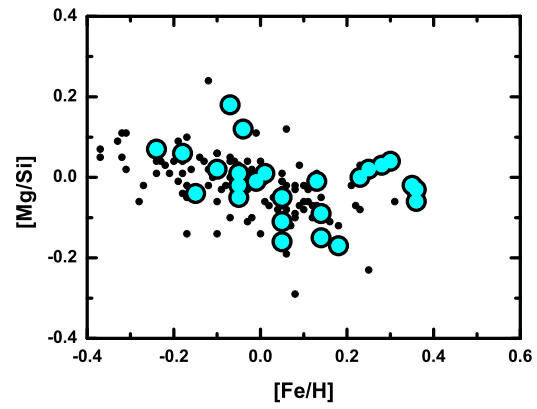
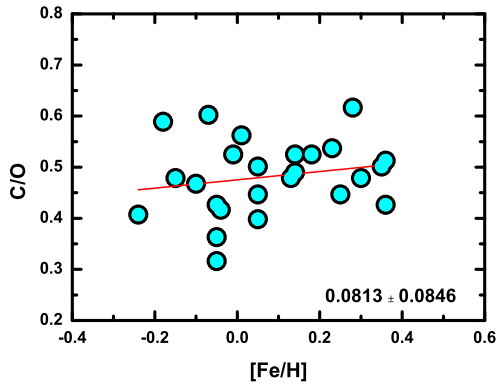


Figure 7.  $[C/H]$ ,  $[C/Fe]$ ,  $[O/H]$ ,  $[O/Fe]$  versus  $[Fe/H]$ .



**Figure 8.**  $[C/O]$ ,  $C/O$  versus  $[Fe/H]$  and  $C/O$  and  $[C/Fe]$  versus planetary mass (in  $M_J$ ).

**Figure 9.**  $[Mg/Si]$  versus  $[Fe/H]$  for stars from Mishenina et al. (2016) (dots) and this study (open circles);  $Mg/Si$  versus  $[Fe/H]$  and planetary mass (in  $M_J$ ).

ward abundance trends with  $T_{cond}$  for only four of eight stars hosting super-Earth-like planets. The authors came to a conclusion that there was no clear evidence of the relationship between the volatile-to-refractory abundance ratio and the presence of rocky planets. Later, a different assumption was made in the studies of Adibekyan et al. (2014, 2015), in particular, that the chemical peculiarities (small refractory-to-volatile ratios) of planet-hosting stars could reflect that those stars were older and indicate their inner Galaxy origin. The GCE, the place of birth in the Galaxy and, prob-

ably, stellar age play an important role in using elemental abundance estimates and clarifying their relationship with various parameters. Nissen (2015) concluded that while an unusually low refractory-to-volatile ratio suggests that the relationship between  $[\text{El}/\text{Fe}]$  and  $T_{\text{cond}}$  may be used as a signature of the existence of terrestrial planets around stars, the dependence of  $[\text{El}/\text{Fe}]$  on the stellar age makes it difficult to employ this relationship as such an indicator.

As response to the study by Nissen (2015), Spina, Meléndez & Ramírez (2016) verified whether the chemical evolution of the Galactic disc could explain different observed slopes of elemental abundance with  $T_{\text{cond}}$ . The authors claimed that a wide diversity of those slopes was still observed after subtracting the chemical evolution effect, which could be indicative of some other processes not related to the GCE that might have affected the element- $T_{\text{cond}}$  slopes. They supposed that such a great difference between those slopes reflected the difference of exo-planetary systems themselves and lies in highly dynamic stages of planetary systems during which some portion of the rocky material surrounds the star (e.g., cores of gaseous planets, rocky planets, and planetesimals) and fall onto the central star; but other planetary systems may be subject to quieter processes. Thus, the observed variety of slopes may correspond to a great number of evolutionary paths of matter in the circumstellar discs during the formation of planetary systems. As noted by Tucci Maia et al. (2019), –terrestrial planets (or the core of giant planets) may influence the surface abundance of its host star in two ways: i) the accretion of rocky material (planetary engulfment) enriches the stellar atmosphere in refractories; ii) imprisonment of refractory rich material into rocky objects that deplete the material accreted by the star during its formation.

Since the cores of massive planets can affect the surface content of refractories, we also attempted to compare the volatile and refractory abundance ratios with  $T_{\text{cond}}$  (Lodders 2003) in our sample of stars hosting massive planets, adjusted for the chemical evolution effects; in other words, we subtracted the mean elemental abundances in non-hosting solar twin stars  $\langle[\text{El}/\text{Fe}]\rangle(\text{st})$  from the  $[\text{El}/\text{Fe}]$  ratios in our target stars. The values of  $\langle[\text{El}/\text{Fe}]\rangle(\text{st})$  were taken from Mishenina et al. (2016). In that paper, 33 stars were selected as solar twins for which the average values of the parameters were  $\langle T_{\text{eff}} \rangle = 5800 \pm 100$  K,  $\langle \log g \rangle = 4.40 \pm 0.09$ ,  $\langle [\text{Fe}/\text{H}] \rangle = 0.00 \pm 0.05$ .

In Fig. 10 we plot with solid line the differences between elemental abundances of our target stars and mean values of the solar twins  $\Delta[\text{El}/\text{Fe}](\text{star}) - \langle[\text{El}/\text{Fe}]\rangle(\text{st})$ , and with dashed line  $[\text{El}/\text{Fe}]$  as a function of  $T_{\text{cond}}$ .

We can see that the stars exhibit both positive and negative slope in the dependencies of  $\Delta[\text{El}/\text{Fe}] - T_{\text{cond}}$ , but most of them do not show noticeable tilts to the trend line. Two stars, namely, HD143105 ( $-0.094 \pm 0.039$ ) and HD214823 ( $-0.118 \pm 0.031$ ) show negative slopes that represent decreasing refractory-to-volatile abundance ratios, and three stars, namely, HD24040 ( $-0.075 \pm 0.061$ ), HD35759 ( $-0.101 \pm 0.074$ ), HD113337 ( $-0.066 \pm 0.043$ ) have only slightly decreasing trend. For all the stars with positive slopes, the error in the slope is higher than its value.

What does such a result suggest? The masses in  $M_J$  unit of the first two stars mentioned above are 1.21 and 19.2, re-

spectively, and 4.00, 3.76, and 10.0 for the other three stars, respectively. Four of five stars that exhibit negative slopes are more massive than  $3 M_J$ . Could this indicate some pattern in the formation of the nuclei of massive planets? It is difficult to answer to this question, since our sample also contains other that do not exhibit any trends. Fig.11 displays the relationship between the resulting slopes ( $\Delta[\text{El}/\text{Fe}]$  versus  $T_{\text{cond}}$ ) and planetary masses in  $M_J$  for all stars of our target. We can see a slight trend ( $-0.0044 \pm 0.0022$ ) indicating possible relationship between negative slope and planetary masses. However, when excluding the two most massive planets from the sample the slope of the linear trend changes to  $-0.0038 \pm 0.0045$ , making the dependence insignificant.

## 7 CONCLUSIONS

We have determined the abundances of 25 elements, from Li to Eu, in a sample of stars with detected massive planets with the exception of one target hosting a Neptune-size mass planetary companion. A comparison of the parameters in this study with those reported in other papers has shown a good agreement, which enables us to perform a consistent analysis of planet hosts and a sufficiently high accuracy and reliability of the derived elemental abundances. The C/O abundances for 16 of 25 sample stars were calculated for the first time; these elements play an important role in the formation of massive planets. We have analyzed the behavior of elemental abundances as a function of various parameters, such as  $[\text{Fe}/\text{H}]$  and  $T_{\text{cond}}$ , and planetary masses. This study has yielded the following findings:

i) The resulting trends of  $[\text{C}/\text{Fe}]$  and  $[\text{O}/\text{Fe}]$  vs.  $[\text{Fe}/\text{H}]$  are consistent with those in the Galactic disc. Our mean values of C/O and  $[\text{C}/\text{O}]$  are  $\langle \text{C}/\text{O} \rangle = 0.48 \pm 0.07$  and  $\langle [\text{C}/\text{O}] \rangle = -0.07 \pm 0.07$ , which are slightly lower than the solar ones. Different individual values of C/O ratios obtained in this study are consistent with a large variance of the C and O abundances in stars hosting massive planetary systems; it does not support the claim that stars with massive planets must be carbon rich, but reflects the fact that the stars in our sample have lower carbon abundances as compared to that in the Sun.

ii) The trend of  $[\text{Mg}/\text{Si}]$  vs.  $[\text{Fe}/\text{H}]$  follows the behaviour of Mg and Si in the Galactic disc. The Mg/Si ratios obtained in this study range from 0.83 to 0.96 for four stars and from 1.0 to 1.86 for the remaining 21 stars in our sample. These results agree well with the study by Suárez-Andrés et al. (2018), in which it was found that 85% stars with high-mass companions had the Mg/Si ratios ranging between one and two;

iii) A trend of  $M_{\text{pl}}$  with  $[\text{Fe}/\text{H}]$  and just a trace of trend representing decreasing Mg/Si ratios with increasing planetary mass have been detected;

iv) The diversity of the observed abundance- $T_{\text{cond}}$  slopes found for planet-hosting stars might be associated with various processes, such as a variety of evolutionary paths of circumstellar discs, accretion or formation of the giant-planet rocky core. However, we cannot rule out that there is no physical relation between presence of planets and the  $T_{\text{cond}}$  trend.

The data obtained in this study can impose constraints on existing models of planetary evolution and prove useful



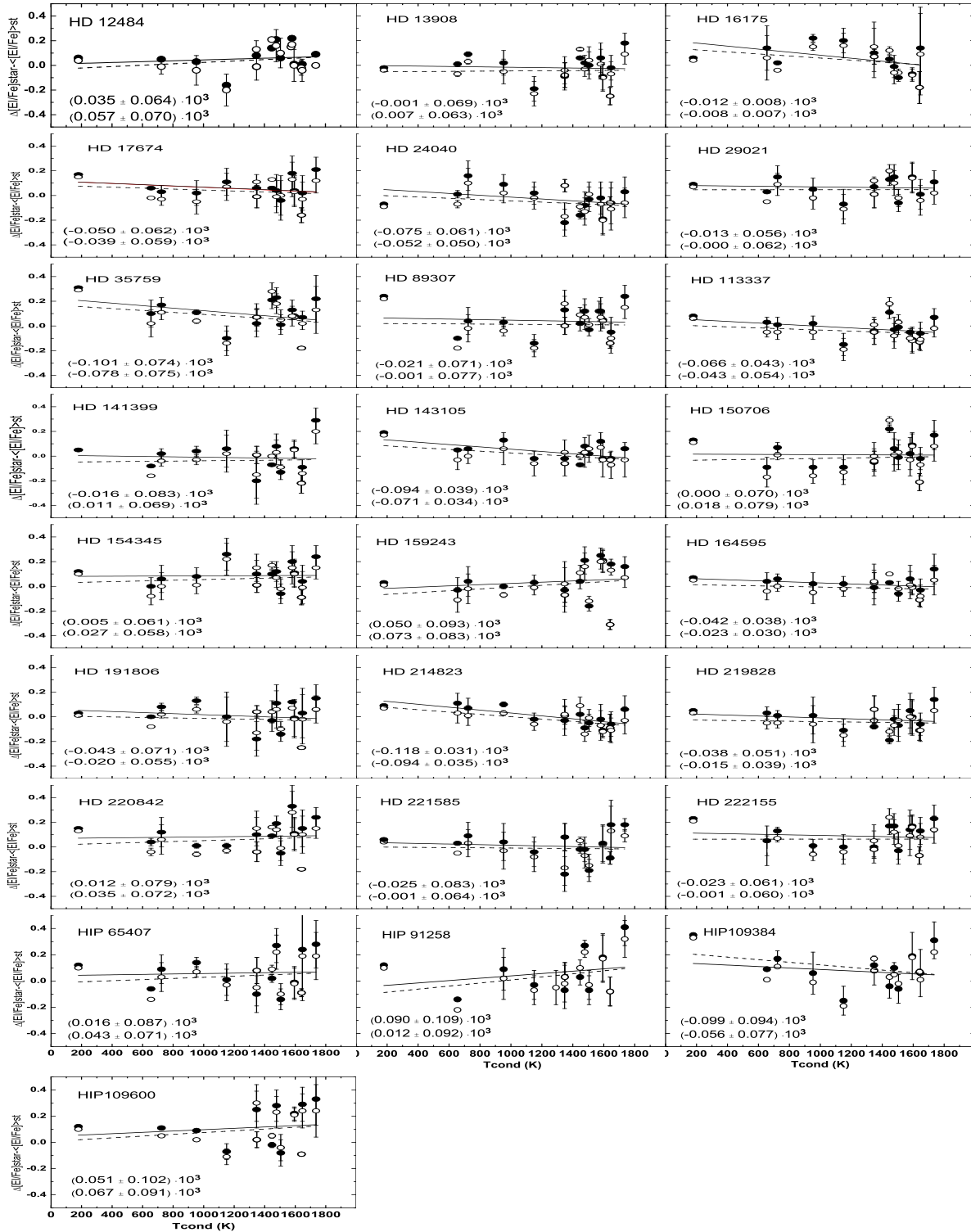


**Figure 10.**  $\Delta[El/Fe]$  and  $[El/Fe]$  versus  $T_{cond}$  for all target stars. The solid and dashed lines correspond to the abundance values with and without corrections, respectively, as well as the numbers indicated in each panel give (upper value with correction, lower value without correction)

in the development and validation of theoretical studies of the formation and evolution of massive planetary systems.

#### DATA AVAILABILITY STATEMENT

The data that support the findings of this study are available from the corresponding author T. Mishenina upon reasonable request.

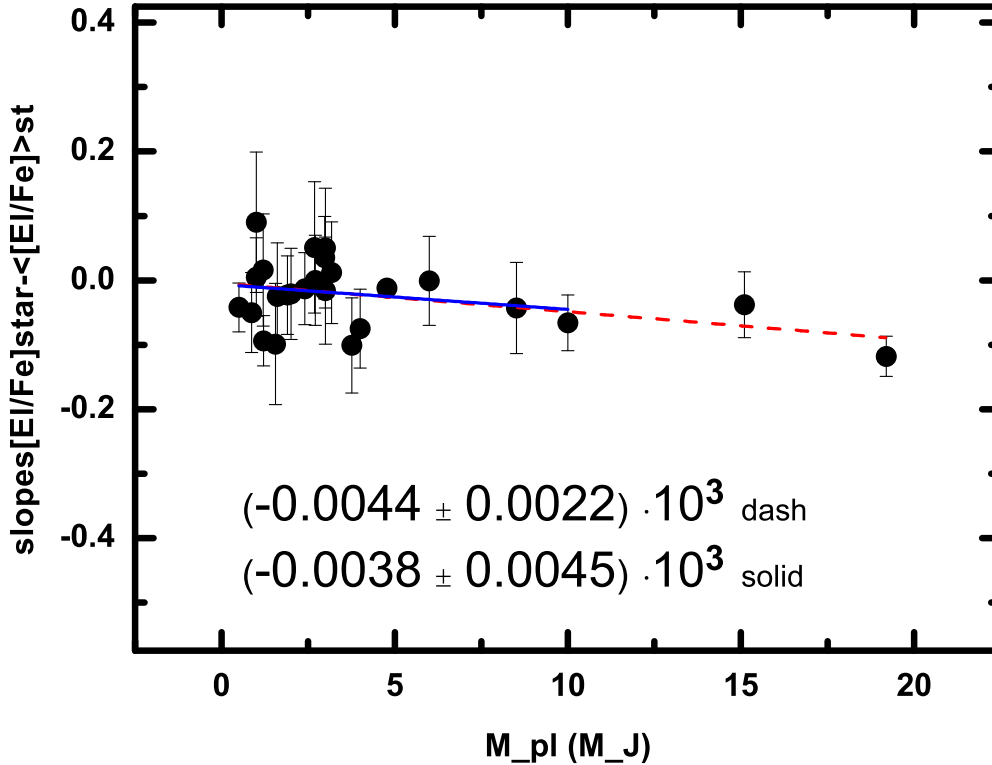


Figure 11. Dependence of the  $\Delta[\text{E}/\text{Fe}]_{-T_{\text{cond}}}$  slope on the planetary mass in  $M_J$

## ACKNOWLEDGEMENTS

The authors thank the anonymous referee for a careful reading of the manuscript and suggestions that significantly improved the manuscript. The authors are grateful to Sergey Korotin for the discussion on the barium abundance. V.A. was supported by FCT - Fundação para a Ciência e Tecnologia (FCT) through national funds and by FEDER through COMPETE2020 - Programa Operacional Competitividade e Internacionalização by these grants: UID/FIS/04434/2019; UIDB/04434/2020; UIDP/04434/2020; PTDC/FIS-AST/32113/2017 & POCI-01-0145-FEDER-032113; PTDC/FIS-AST/28953/2017 & POCI-01-0145-FEDER-028953. V.A. also acknowledges the support from FCT through Investigador FCT contracts nr. IF/00650/2015/CP1273/CT0001, and POPH/FSE (EC) by FEDER funding through the program “Programa Operacional de Factores de Competitividade - COMPETE”. This article is based upon work from the ChETEC COST Action (CA16117), supported by COST (European Cooperation in Science and Technology).

## REFERENCES

Adibekyan V., 2019, *Geosciences*, 9, 105

- Adibekyan V., Gonçalves da Silva H. M., Sousa S. G., Santos N. C., Delgado Mena E., Hakobyan A. A., 2017, *Astrophysics*, 60, 325
- Adibekyan V. et al., 2015, *A&A*, 581, L2
- Adibekyan V. Z., Delgado Mena E., Sousa S. G., Santos N. C., Israelian G., González Hernández J. I., Mayor M., Hakobyan A. A., 2012a, *A&A*, 547, A36
- Adibekyan V. Z., González Hernández J. I., Delgado Mena E., Sousa S. G., Santos N. C., Israelian G., Figueira P., Bertran de Lis S., 2014, *A&A*, 564, L15
- Adibekyan V. Z., Sousa S. G., Santos N. C., Delgado Mena E., González Hernández J. I., Israelian G., Mayor M., Khachatryan G., 2012b, *A&A*, 545, A32
- Aguilera-Gómez C., Ramírez I., Chanamé J., 2018, *A&A*, 614, A55
- Andrievsky S. M., Spite M., Korotin S. A., Spite F., Bonifacio P., Cayrel R., Hill V., François P., 2008, *A&A*, 481, 481
- Asplund M., Grevesse N., Sauval A. J., Scott P., 2009, *ARA&A*, 47, 481
- Baraffe I., Pratt J., Goffrey T., Constantino T., Folini D., Popov M. V., Walder R., Viallet M., 2017, *ApJ*, 845, L6
- Baumann P., Ramírez I., Meléndez J., Asplund M., Lind K., 2010, *A&A*, 519, A87
- Beck P. G. et al., 2017, *A&A*, 602, A63
- Boisse I. et al., 2012, *A&A*, 545, A55
- Bond J. C., O’Brien D. P., Lauretta D. S., 2010, *ApJ*, 715,



- 1050
- Borgniet S. et al., 2019, *A&A*, 621, A87
- Bouchy F. et al., 2009, *A&A*, 505, 853
- Bouvier J. et al., 2016, *A&A*, 590, A78
- Brewer J. M., Fischer D. A., Valenti J. A., Piskunov N., 2016, *ApJS*, 225, 32
- Caffau E., Ludwig H. G., Bonifacio P., Faraggiana R., Stefan M., Freytag B., Kamp I., Ayres T. R., 2010, *A&A*, 514, A92
- Carlos M., Nissen P. E., Meléndez J., 2016, *A&A*, 587, A100
- Castelli F., Kurucz R. L., 2004, *ArXiv Astrophysics e-prints*
- Courcol B. et al., 2015, *A&A*, 581, A38
- da Silva R., Milone A. C., Reddy B. E., 2011, *A&A*, 526, A71
- da Silva R., Milone A. d. C., Rocha-Pinto H. J., 2015, *A&A*, 580, A24
- Delgado Mena E. et al., 2015, *A&A*, 576, A69
- Delgado Mena E., Israelian G., González Hernández J. I., Bond J. C., Santos N. C., Udry S., Mayor M., 2010, *ApJ*, 725, 2349
- Delgado Mena E. et al., 2014, *A&A*, 562, A92
- Díaz R. F. et al., 2016, *A&A*, 591, A146
- Ecuivillon A., Israelian G., Santos N. C., Mayor M., Gilli G., 2006, *A&A*, 449, 809
- Figueira P., Faria J. P., Delgado-Mena E., Adibekyan V. Z., Sousa S. G., Santos N. C., Israelian G., 2014, *A&A*, 570, A21
- Fischer D. A., Valenti J., 2005, *ApJ*, 622, 1102
- Gonzalez G., 1997, *MNRAS*, 285, 403
- Gonzalez G., 1998, *A&A*, 334, 221
- Gonzalez G., 2008, *MNRAS*, 386, 928
- Gonzalez G., Carlson M. K., Tobin R. W., 2010, *MNRAS*, 403, 1368
- Gonzalez G., Laws C., 2000, *AJ*, 119, 390
- González Hernández J. I., Delgado-Mena E., Sousa S. G., Israelian G., Santos N. C., Adibekyan V. Z., Udry S., 2013, *A&A*, 552, A6
- Grevesse N., Asplund M., Sauval A. J., 2007, *Space Sci. Rev.*, 130, 105
- Guillot T., 2005, *Annual Review of Earth and Planetary Sciences*, 33, 493
- Hébrard G. et al., 2016, *A&A*, 588, A145
- Israelian G. et al., 2009, *Nature*, 462, 189
- Israelian G., Santos N. C., Mayor M., Rebolo R., 2001, *Nature*, 411, 163
- Israelian G., Santos N. C., Mayor M., Rebolo R., 2004, *A&A*, 414, 601
- Ivans I. I., Simmerer J., Sneden C., Lawler J. E., Cowan J. J., Gallino R., Bisterzo S., 2006, *ApJ*, 645, 613
- Jofré E., Petrucci R., Saffe C., Saker L., Artur de la Vilharmois E., Chavero C., Gómez M., Mauas P. J. D., 2015, *A&A*, 574, A50
- Johansson S., Litzén U., Lundberg H., Zhang Z., 2003, *ApJ*, 584, L107
- Käppeler F., Gallino R., Bisterzo S., Aoki W., 2011, *Reviews of Modern Physics*, 83, 157
- Katsova M. M., Livshits M. A., Mishenina T. V., 2013, *Astronomy Reports*, 57, 702
- Korotin S., Mishenina T., Gorbaneva T., Soubiran C., 2011, *MNRAS*, 415, 2093
- Korotin S. A., Andrievsky S. M., Hansen C. J., Caffau E., Bonifacio P., Spite M., Spite F., François P., 2015, *A&A*, 581, A70
- Korotin S. A., Andrievsky S. M., Luck R. E., Lépine J. R. D., Maciel W. J., Kovtyukh V. V., 2014, *MNRAS*, 444, 3301
- Kovtyukh V. V., Soubiran C., Belik S. I., Gorlova N. I., 2003, *A&A*, 411, 559
- Kuchner M. J., Seager S., 2005, *arXiv e-prints, astro*
- Kupka F., Piskunov N., Ryabchikova T. A., Stempels H. C., Weiss W. W., 1999, *A&AS*, 138, 119
- Lind K., Asplund M., Barklem P. S., 2009, *A&A*, 503, 541
- Lodders K., 2003, *ApJ*, 591, 1220
- Maeder A., Meynet G., 2012, *Reviews of Modern Physics*, 84, 25
- Mashonkina L., Gehren T., 2000, *A&A*, 364, 249
- Meléndez J., Asplund M., Gustafsson B., Yong D., 2009, *ApJ*, 704, L66
- Mishenina T., Gorbaneva T., Pignatari M., Thielemann F. K., Korotin S. A., 2015, *MNRAS*, 454, 1585
- Mishenina T., Kovtyukh V., Soubiran C., Adibekyan V. Z., 2016, *MNRAS*, 462, 1563
- Mishenina T. et al., 2017, *MNRAS*, 469, 4378
- Mishenina T. V., Korotin S. A., Klochkova V. G., Panchuk V. E., 2000, *A&A*, 353, 978
- Mishenina T. V., Soubiran C., Kovtyukh V. V., Katsova M. M., Livshits M. A., 2012, *A&A*, 547, A106
- Mishenina T. V., Soubiran C., Kovtyukh V. V., Korotin S. A., 2004, *A&A*, 418, 551
- Mishenina T. V., Tsymbal V. V., 1997, *Astronomy Letters*, 23, 609
- Montalbán J., Rebolo R., 2002, *A&A*, 386, 1039
- Mortier A., Santos N. C., Sozzetti A., Mayor M., Latham D., Bonfils X., Udry S., 2012, *A&A*, 543, A45
- Moultaka J., Ilovaisky S., Prugniel P., Soubiran C., 2004, in *SF2A-2004: Semaine de l'Astrophysique Française*, Combes F., Barret D., Contini T., Meynadier F., Pagani L., eds., p. 547
- Moutou C. et al., 2014, *A&A*, 563, A22
- Nissen P. E., 2013, *A&A*, 552, A73
- Nissen P. E., 2015, *A&A*, 579, A52
- Nissen P. E., Chen Y. Q., Carigi L., Schuster W. J., Zhao G., 2014, *A&A*, 568, A25
- Nissen P. E., Christensen-Dalsgaard J., Mosumgaard J. R., Silva Aguirre V., Spitoni E., Verma. K., 2020, *arXiv e-prints, arXiv:2006.06013*
- Nomoto K., Thielemann F. K., Yokoi K., 1984, *ApJ*, 286, 644
- Pavlenko Y. V., Kaminsky B. M., Jenkins J. S., Ivanyuk O. M., Jones H. R. A., Lyubchik Y. P., 2019, *A&A*, 621, A112
- Perruchot S. et al., 2011, in *Society of Photo-Optical Instrumentation Engineers (SPIE) Conference Series*, Vol. 8151, *Techniques and Instrumentation for Detection of Exoplanets V*, Shaklan S., ed., p. 815115
- Petigura E. A., Marcy G. W., 2011, *ApJ*, 735, 41
- Prantzos N., Abia C., Limongi M., Chieffi A., Cristallo S., 2018, *MNRAS*, 476, 3432
- Prochaska J. X., McWilliam A., 2000, *ApJ*, 537, L57
- Queloz D., Allain S., Mermilliod J. C., Bouvier J., Mayor M., 1998, *A&A*, 335, 183
- Ramírez I., Fish J. R., Lambert D. L., Allende Prieto C., 2012, *ApJ*, 756, 46

- Rey J. et al., 2017, *A&A*, 601, A9
- Santos N. C., Israelian G., Mayor M., 2001, *A&A*, 373, 1019
- Santos N. C. et al., 2016, *A&A*, 592, A13
- Santos N. C. et al., 2013, *A&A*, 556, A150
- Smith V. V., Cunha K., Lazzaro D., 2001, *AJ*, 121, 3207
- Sousa S. G. et al., 2008, *A&A*, 487, 373
- Sousa S. G. et al., 2015, *A&A*, 576, A94
- Spina L., Meléndez J., Ramírez I., 2016, *A&A*, 585, A152
- Stonkutė E. et al., 2020, *AJ*, 159, 90
- Suárez-Andrés L., Israelian G., González Hernández J. I., Adibekyan V. Z., Delgado Mena E., Santos N. C., Sousa S. G., 2016, *A&A*, 591, A69
- Suárez-Andrés L., Israelian G., González Hernández J. I., Adibekyan V. Z., Delgado Mena E., Santos N. C., Sousa S. G., 2017, *A&A*, 599, A96
- Suárez-Andrés L., Israelian G., González Hernández J. I., Adibekyan V. Z., Delgado Mena E., Santos N. C., Sousa S. G., 2018, *A&A*, 614, A84
- Takeda Y., Kawanomoto S., 2005, *PASJ*, 57, 45
- Takeda Y., Kawanomoto S., Honda S., Ando H., Sakurai T., 2007, *A&A*, 468, 663
- Teske J. K., Cunha K., Smith V. V., Schuler S. C., Griffith C. A., 2014, *ApJ*, 788, 39
- Thiabaud A., Marboeuf U., Alibert Y., Leya I., Mezger K., 2015a, *A&A*, 580, A30
- Thiabaud A., Marboeuf U., Alibert Y., Leya I., Mezger K., 2015b, *A&A*, 574, A138
- Thorburn J. A., Hobbs L. M., Deliyannis C. P., Pinsonneault M. H., 1993, *ApJ*, 415, 150
- Timmes F. X., Woosley S. E., Weaver T. A., 1995, *ApJS*, 98, 617
- Tsymbol V., 1996, in *Astronomical Society of the Pacific Conference Series*, Vol. 108, M.A.S.S., *Model Atmospheres and Spectrum Synthesis*, Adelman S. J., Kupka F., Weiss W. W., eds., p. 198
- Tucci Maia M., Meléndez J., Lorenzo-Oliveira D., Spina L., Jofré P., 2019, *A&A*, 628, A126
- Udry S., Santos N. C., 2007, *ARA&A*, 45, 397
- Woosley S. E., Weaver T. A., 1995, *ApJS*, 101, 181

## APPENDIX A: ON-LINE MATERIAL

Table A1: The list of used lines

Wave	Ion	Elow	log $gf$	Wave	Ion	Elow	log $gf$	Wave	Ion	Elow	log $gf$
5688.205	11.00	2.104	-0.451	5653.867	26.00	4.387	-1.639	6739.522	26.00	1.557	-4.793
6154.226	11.00	2.102	-1.546	5661.346	26.00	4.284	-1.735	6745.101	26.00	4.580	-2.159
6160.747	11.00	2.104	-1.245	5672.264	26.00	4.584	-2.799	6745.957	26.00	4.076	-2.769
4571.096	12.00	0.000	-5.622	5678.379	26.00	3.884	-3.019	6746.955	26.00	2.609	-4.349
4730.029	12.00	4.346	-2.346	5679.023	26.00	4.652	-0.919	6750.153	26.00	2.424	-2.620
5711.088	12.00	4.346	-1.723	5680.240	26.00	4.186	-2.579	6752.707	26.00	4.638	-1.203
6318.717	12.00	5.108	-2.102	5686.530	26.00	4.549	-0.445	6753.464	26.00	4.559	-2.289
6319.237	12.00	5.108	-2.323	5691.497	26.00	4.301	-1.519	6761.070	26.00	4.584	-2.529
6319.493	12.00	5.108	-2.802	5698.020	26.00	3.640	-2.679	6764.107	26.00	4.593	-2.787
6696.023	13.00	3.143	-1.346	5701.545	26.00	2.559	-2.215	6769.659	26.00	4.580	-2.659
6698.673	13.00	3.143	-1.646	5705.465	26.00	4.301	-1.354	6783.704	26.00	2.588	-3.979
5645.613	14.00	4.930	-2.139	5707.050	26.00	3.642	-2.399	6786.860	26.00	4.191	-2.069
5665.554	14.00	4.920	-2.039	5717.833	26.00	4.284	-1.129	6793.259	26.00	4.076	-2.325
5690.425	14.00	4.930	-1.869	5720.898	26.00	4.549	-1.949	6794.619	26.00	4.956	-2.109
5772.146	14.00	5.082	-1.749	5724.455	26.00	4.284	-2.639	6796.125	26.00	4.143	-2.529
5793.073	14.00	4.930	-2.059	5731.762	26.00	4.256	-1.299	6801.865	26.00	1.608	-4.734
5948.541	14.00	5.082	-1.229	5732.296	26.00	4.991	-1.559	6806.845	26.00	2.728	-3.209
6125.021	14.00	5.614	-1.464	5732.863	26.00	4.103	-3.039	6810.263	26.00	4.607	-0.985
6142.483	14.00	5.619	-1.295	5738.228	26.00	4.220	-2.339	6820.372	26.00	4.638	-1.319
6145.016	14.00	5.616	-1.310	5741.848	26.00	4.256	-1.853	6824.823	26.00	4.988	-2.129
6243.815	14.00	5.616	-1.243	5752.032	26.00	4.549	-1.176	6828.591	26.00	4.638	-0.919
6244.465	14.00	5.616	-1.090	5753.123	26.00	4.260	-0.687	6833.226	26.00	4.638	-2.079
6741.628	14.00	5.984	-1.749	5759.262	26.00	4.652	-2.069	6837.006	26.00	4.593	-1.686
6748.790	16.00	7.868	-0.529	5760.345	26.00	3.642	-2.489	6839.831	26.00	2.559	-3.449
6757.150	16.00	7.870	-0.239	5762.414	26.00	3.642	-2.279	6841.339	26.00	4.607	-0.749
4578.551	20.00	2.521	-0.696	5762.992	26.00	4.209	-0.449	6842.686	26.00	4.638	-1.319
4685.268	20.00	2.933	-0.878	5775.081	26.00	4.220	-1.297	6843.656	26.00	4.549	-0.929
5349.465	20.00	2.709	-0.309	5778.453	26.00	2.588	-3.429	6855.162	26.00	4.559	-0.741
5581.965	20.00	2.523	-0.554	5793.915	26.00	4.220	-1.699	6855.713	26.00	4.607	-1.819
5590.114	20.00	2.521	-0.570	5804.035	26.00	3.882	-2.289	6857.250	26.00	4.076	-2.149
5601.277	20.00	2.526	-0.522	5806.725	26.00	4.608	-1.049	6858.150	26.00	4.608	-0.929
5867.562	20.00	2.933	-1.569	5809.218	26.00	3.884	-1.839	6862.480	26.00	4.559	-1.569
6122.217	20.00	1.886	-0.315	5811.915	26.00	4.143	-2.429	6864.311	26.00	4.559	-2.319
6166.439	20.00	2.521	-1.141	5814.808	26.00	4.283	-1.969	4893.820	26.01	2.828	-4.266
6439.075	20.00	2.526	0.390	5816.374	26.00	4.549	-0.600	4993.358	26.01	2.807	-3.639
6471.662	20.00	2.526	-0.685	5826.638	26.00	4.283	-2.939	5100.664	26.01	2.807	-4.169
6717.681	20.00	2.709	-0.523	5827.877	26.00	3.283	-3.409	5132.669	26.01	2.807	-3.979
5201.080	22.00	2.092	-0.659	5835.101	26.00	4.256	-2.369	5197.577	26.01	3.230	-2.099
5210.385	22.00	0.048	-0.849	5837.701	26.00	4.294	-2.339	5234.625	26.01	3.221	-2.229
5219.701	22.00	0.021	-2.259	5838.372	26.00	3.943	-2.339	5256.937	26.01	2.891	-4.181
5223.620	22.00	2.092	-0.489	5845.287	26.00	5.033	-1.819	5325.553	26.01	3.221	-3.119
5224.300	22.00	2.134	0.130	5849.684	26.00	3.695	-2.989	5362.869	26.01	3.199	-2.615
5282.376	22.00	1.053	-1.299	5852.219	26.00	4.549	-1.329	5414.073	26.01	3.221	-3.539
5295.775	22.00	1.067	-1.632	5855.077	26.00	4.608	-1.477	5425.257	26.01	3.199	-3.159
5300.011	22.00	1.053	-1.469	5856.088	26.00	4.294	-1.327	5534.847	26.01	3.245	-2.729
5338.305	22.00	0.826	-1.869	5858.778	26.00	4.220	-2.259	5627.497	26.01	3.387	-4.129
5426.250	22.00	0.021	-3.005	5859.586	26.00	4.549	-0.418	5725.963	26.01	3.425	-4.819
5490.148	22.00	1.460	-0.932	5861.110	26.00	4.283	-2.449	5732.724	26.01	3.387	-4.635
5648.565	22.00	2.495	-0.259	5862.356	26.00	4.549	-0.126	5823.155	26.01	5.569	-2.986
5689.460	22.00	2.297	-0.359	5864.244	26.00	4.301	-2.519	5932.055	26.01	3.199	-5.049
5866.451	22.00	1.067	-0.839	5873.213	26.00	4.256	-2.139	5991.376	26.01	3.153	-3.539
5899.294	22.00	1.053	-1.153	5877.788	26.00	4.178	-2.229	6084.111	26.01	3.199	-3.779
5918.535	22.00	1.067	-1.459	5879.487	26.00	4.607	-2.139	6113.322	26.01	3.221	-4.109
5922.109	22.00	1.046	-1.465	5880.027	26.00	4.559	-1.939	6129.703	26.01	3.199	-4.739
5937.809	22.00	1.067	-1.889	5881.280	26.00	4.608	-1.839	6149.258	26.01	3.889	-2.719
5953.160	22.00	1.887	-0.328	5883.817	26.00	3.960	-1.359	6179.384	26.01	5.569	-2.796
5965.828	22.00	1.879	-0.408	5902.474	26.00	4.593	-1.809	6233.534	26.01	5.484	-2.831
5978.541	22.00	1.873	-0.495	5905.672	26.00	4.652	-0.729	6238.392	26.01	3.889	-2.753
6091.171	22.00	2.267	-0.422	5909.974	26.00	3.211	-2.586	6239.953	26.01	3.889	-3.572

Table A1: The list of used lines

Wave	Ion	Elow	log <i>gf</i>	Wave	Ion	Elow	log <i>gf</i>	Wave	Ion	Elow	log <i>gf</i>
6121.001	22.00	1.879	-0.966	5916.247	26.00	2.453	-2.993	6247.557	26.01	3.892	-2.309
6126.216	22.00	1.067	-1.424	5927.789	26.00	4.652	-1.089	6248.898	26.01	5.511	-2.783
6258.102	22.00	1.443	-0.354	5930.180	26.00	4.652	-0.229	6369.462	26.01	2.891	-4.159
6258.706	22.00	1.460	-0.239	5934.655	26.00	3.929	-1.169	6383.722	26.01	5.553	-2.069
6261.097	22.00	1.430	-0.478	5956.694	26.00	0.859	-4.604	6407.251	26.01	3.889	-3.853
5211.530	22.01	2.590	-1.159	5975.350	26.00	4.835	-0.691	6416.919	26.01	3.892	-2.649
5268.615	22.01	2.598	-1.669	5976.777	26.00	3.943	-1.242	6432.680	26.01	2.891	-3.519
5396.226	22.01	1.584	-3.019	5983.680	26.00	4.549	-1.467	6442.955	26.01	5.549	-2.670
5418.751	22.01	1.582	-2.109	5984.815	26.00	4.733	-0.195	6446.410	26.01	6.223	-1.959
6606.950	22.01	2.061	-2.789	5987.065	26.00	4.796	-0.428	6516.080	26.01	2.891	-3.319
5214.131	24.00	3.369	-0.739	6003.012	26.00	3.882	-1.119	5388.344	28.00	1.935	-3.559
5247.565	24.00	0.961	-1.589	6007.960	26.00	4.652	-0.596	5392.331	28.00	4.154	-1.319
5272.000	24.00	3.449	-0.419	6008.556	26.00	3.884	-0.985	5424.645	28.00	1.951	-2.769
5287.178	24.00	3.438	-0.869	6018.299	26.00	4.652	-2.081	5435.858	28.00	1.986	-2.589
5297.377	24.00	2.900	0.209	6024.058	26.00	4.549	-0.119	5452.861	28.00	3.796	-1.659
5304.180	24.00	3.464	-0.669	6027.051	26.00	4.076	-1.088	5453.230	28.00	4.088	-1.489
5312.856	24.00	3.449	-0.549	6054.074	26.00	4.371	-2.309	5462.493	28.00	3.847	-0.929
5329.138	24.00	2.914	-0.007	6056.005	26.00	4.733	-0.459	5494.880	28.00	4.105	-1.159
5344.757	24.00	3.449	-0.989	6062.848	26.00	2.176	-4.139	5578.718	28.00	1.676	-2.639
5345.796	24.00	1.004	-0.949	6065.482	26.00	2.609	-1.529	5589.358	28.00	3.898	-1.139
5348.315	24.00	1.004	-1.209	6078.491	26.00	4.796	-0.320	5593.735	28.00	3.898	-0.839
5628.643	24.00	3.422	-0.739	6079.009	26.00	4.652	-1.119	5625.317	28.00	4.089	-0.699
5642.358	24.00	3.857	-0.898	6082.711	26.00	2.223	-3.572	5637.119	28.00	4.089	-0.819
5664.579	24.00	3.826	-0.632	6085.259	26.00	2.759	-3.094	5638.820	28.00	3.898	-1.719
5712.771	24.00	3.011	-1.029	6093.644	26.00	4.608	-1.499	5641.881	28.00	4.105	-1.069
5783.063	24.00	3.323	-0.374	6094.374	26.00	4.652	-1.939	5643.078	28.00	4.165	-1.239
5783.850	24.00	3.322	-0.360	6096.665	26.00	3.984	-1.929	5663.985	28.00	4.538	-0.429
5784.969	24.00	3.321	-0.346	6098.245	26.00	4.559	-1.879	5682.199	28.00	4.105	-0.469
5787.918	24.00	3.322	-0.049	6102.171	26.00	4.835	-0.515	5694.983	28.00	4.089	-0.609
6330.091	24.00	0.941	-2.919	6105.131	26.00	4.549	-2.049	5748.351	28.00	1.676	-3.259
6661.075	24.00	4.193	-0.112	6120.249	26.00	0.915	-5.949	5754.656	28.00	1.935	-2.329
6882.512	24.00	3.438	-0.310	6127.907	26.00	4.143	-1.398	5760.830	28.00	4.105	-0.799
6883.052	24.00	3.438	-0.355	6136.615	26.00	2.453	-1.399	5805.217	28.00	4.167	-0.639
4892.859	26.00	4.218	-1.289	6137.692	26.00	2.588	-1.402	5831.595	28.00	4.167	-0.944
4917.230	26.00	4.191	-1.179	6151.618	26.00	2.176	-3.298	5846.993	28.00	1.676	-3.209
4924.770	26.00	2.279	-2.240	6157.728	26.00	4.076	-1.259	5996.730	28.00	4.236	-1.059
4950.106	26.00	3.417	-1.669	6159.378	26.00	4.608	-1.969	6007.310	28.00	1.676	-3.329
4973.102	26.00	3.960	-0.949	6165.360	26.00	4.143	-1.473	6039.298	28.00	4.236	-2.029
4994.130	26.00	0.915	-3.079	6170.507	26.00	4.796	-0.439	6086.281	28.00	4.266	-0.529
5029.618	26.00	3.415	-2.049	6173.336	26.00	2.223	-2.879	6108.116	28.00	1.676	-2.449
5044.211	26.00	2.851	-2.037	6180.204	26.00	2.728	-2.585	6111.070	28.00	4.088	-0.869
5049.820	26.00	2.279	-1.354	6187.990	26.00	3.943	-1.719	6128.973	28.00	1.676	-3.329
5056.841	26.00	4.260	-1.959	6200.313	26.00	2.609	-2.436	6130.135	28.00	4.266	-0.959
5067.150	26.00	4.220	-0.969	6209.714	26.00	3.960	-3.248	6176.807	28.00	4.088	-0.259
5072.672	26.00	4.220	-0.836	6213.430	26.00	2.223	-2.481	6186.711	28.00	4.105	-0.959
5083.339	26.00	0.958	-2.957	6215.144	26.00	4.186	-1.319	6204.600	28.00	4.088	-1.099
5090.774	26.00	4.256	-0.399	6219.281	26.00	2.198	-2.432	6223.981	28.00	4.105	-0.909
5126.193	26.00	4.256	-1.079	6220.784	26.00	3.882	-2.459	6230.089	28.00	4.105	-1.259
5133.689	26.00	4.178	0.140	6226.736	26.00	3.884	-2.219	6259.595	28.00	4.089	-1.236
5171.596	26.00	1.485	-1.792	6229.228	26.00	2.845	-2.804	6327.598	28.00	1.676	-3.149
5198.711	26.00	2.223	-2.134	6230.723	26.00	2.559	-1.280	6360.811	28.00	4.167	-1.026
5215.181	26.00	3.266	-0.870	6232.641	26.00	3.654	-1.222	6366.480	28.00	4.167	-0.873
5216.274	26.00	1.608	-2.149	6240.646	26.00	2.223	-3.232	6378.247	28.00	4.154	-0.829
5217.389	26.00	3.211	-1.069	6246.319	26.00	3.603	-0.732	6424.852	28.00	4.167	-1.354
5242.491	26.00	3.634	-0.966	6252.555	26.00	2.404	-1.686	6532.873	28.00	1.935	-3.389
5243.777	26.00	4.256	-1.149	6254.259	26.00	2.279	-2.442	6586.310	28.00	1.951	-2.809
5257.655	26.00	3.573	-2.752	6265.134	26.00	2.176	-2.549	6598.598	28.00	4.236	-0.979
5281.790	26.00	3.039	-0.833	6270.225	26.00	2.858	-2.463	6767.772	28.00	1.826	-2.169
5288.525	26.00	3.695	-1.507	6271.279	26.00	3.332	-2.702	6772.315	28.00	3.658	-0.979

Table A1: The list of used lines

Wave	Ion	Elow	log $gf$	Wave	Ion	Elow	log $gf$	Wave	Ion	Elow	log $gf$
5307.361	26.00	1.608	-2.986	6290.965	26.00	4.733	-0.773	6842.037	28.00	3.658	-1.479
5324.179	26.00	3.211	-0.102	6297.793	26.00	2.223	-2.739	6850.480	28.00	3.679	-2.099
5326.143	26.00	3.573	-2.070	6322.686	26.00	2.588	-2.425	4680.134	30.00	4.006	-0.814
5339.929	26.00	3.266	-0.646	6330.850	26.00	4.733	-1.739	4722.153	30.00	4.030	-0.337
5364.871	26.00	4.446	0.228	6335.331	26.00	2.198	-2.176	4810.528	30.00	4.078	-0.136
5365.399	26.00	3.573	-1.019	6336.824	26.00	3.686	-0.855	6362.338	30.00	5.796	0.150
5367.467	26.00	4.415	0.443	6344.149	26.00	2.433	-2.922	5119.112	39.01	0.992	-1.359
5373.709	26.00	4.473	-0.859	6355.029	26.00	2.845	-2.349	5289.815	39.01	1.033	-1.849
5379.574	26.00	3.695	-1.513	6358.698	26.00	0.859	-4.467	5402.774	39.01	1.839	-0.629
5383.369	26.00	4.313	0.645	6364.366	26.00	4.796	-1.429	5509.895	39.01	0.992	-0.947
5389.479	26.00	4.415	-0.409	6380.743	26.00	4.186	-1.375	5728.887	39.01	1.839	-1.658
5391.459	26.00	4.154	-0.781	6392.539	26.00	2.279	-4.029	6795.414	39.01	1.738	-1.029
5393.168	26.00	3.241	-0.714	6393.601	26.00	2.433	-1.431	5112.270	40.01	1.665	-0.849
5398.279	26.00	4.446	-0.669	6408.018	26.00	3.686	-1.017	5350.089	40.01	1.827	-1.239
5405.775	26.00	0.990	-1.843	6411.649	26.00	3.654	-0.594	5350.350	40.01	1.773	-1.159
5410.910	26.00	4.473	0.398	6419.950	26.00	4.733	-0.239	4486.909	58.01	0.295	-0.179
5415.199	26.00	4.387	0.642	6421.351	26.00	2.279	-2.026	4562.359	58.01	0.478	0.210
5417.033	26.00	4.415	-1.679	6430.846	26.00	2.176	-2.005	5044.023	58.01	1.212	-0.139
5424.068	26.00	4.320	0.520	6436.407	26.00	4.186	-2.459	5117.169	58.01	1.402	-0.049
5434.524	26.00	1.011	-2.121	6469.193	26.00	4.835	-0.769	5252.661	58.01	1.155	-0.639
5445.042	26.00	4.387	-0.019	6475.624	26.00	2.559	-2.941	5274.229	58.01	1.044	0.130
5452.088	26.00	3.640	-2.859	6481.870	26.00	2.279	-2.983	5330.556	58.01	0.869	-0.399
5464.280	26.00	4.143	-1.401	6494.981	26.00	2.404	-1.272	5472.279	58.01	1.247	-0.099
5466.396	26.00	4.371	-0.629	6495.742	26.00	4.835	-0.939	5518.489	58.01	1.155	-0.649
5497.516	26.00	1.011	-2.848	6498.939	26.00	0.958	-4.698	6043.373	58.01	1.206	-0.479
5501.465	26.00	0.958	-3.046	6518.367	26.00	2.832	-2.459	5110.763	59.01	1.148	0.320
5506.779	26.00	0.990	-2.796	6533.929	26.00	4.559	-1.459	5219.045	59.01	0.795	-0.052
5522.447	26.00	4.209	-1.549	6592.914	26.00	2.728	-1.472	5259.728	59.01	0.633	0.114
5531.984	26.00	4.913	-1.609	6593.871	26.00	2.433	-2.421	5322.771	59.01	0.483	-0.318
5543.150	26.00	3.695	-1.569	6597.561	26.00	4.796	-1.069	5352.404	59.01	0.483	-0.652
5554.895	26.00	4.549	-0.439	6608.026	26.00	2.279	-4.029	6397.973	59.01	1.053	-0.939
5560.212	26.00	4.435	-1.189	6609.110	26.00	2.559	-2.691	4959.120	60.01	0.064	-0.799
5565.704	26.00	4.608	-0.212	6627.545	26.00	4.549	-1.679	5092.790	60.01	0.380	-0.609
5572.842	26.00	3.397	-0.274	6646.932	26.00	2.609	-3.989	5130.590	60.01	1.304	0.450
5576.089	26.00	3.430	-0.999	6653.853	26.00	4.154	-2.519	5181.169	60.01	0.859	-0.599
5584.765	26.00	3.573	-2.319	6677.987	26.00	2.692	-1.417	5319.810	60.01	0.550	-0.139
5586.756	26.00	3.368	-0.119	6699.142	26.00	4.593	-2.100	5431.520	60.01	1.121	-0.469
5633.947	26.00	4.991	-0.269	6703.567	26.00	2.759	-3.159	5740.860	60.01	1.160	-0.529
5635.823	26.00	4.256	-1.889	6704.481	26.00	4.218	-2.659	5842.366	60.01	1.282	-0.599
5636.696	26.00	3.640	-2.609	6705.101	26.00	4.607	-1.391	6740.078	60.01	0.064	-2.099
5638.262	26.00	4.220	-0.869	6713.745	26.00	4.796	-1.599	4642.230	62.01	0.378	-0.459
5641.434	26.00	4.256	-1.179	6715.383	26.00	4.608	-1.639	4676.900	62.01	0.040	-0.869
5646.684	26.00	4.260	-2.499	6716.237	26.00	4.580	-1.919	4815.800	62.01	0.185	-0.819
5649.987	26.00	5.100	-0.919	6725.357	26.00	4.103	-2.299	4952.370	62.01	0.333	-1.249
5650.706	26.00	5.086	-0.959	6726.666	26.00	4.607	-1.132	4972.170	62.01	0.933	-0.939
5651.469	26.00	4.473	-1.999	6733.151	26.00	4.638	-1.579	6731.810	62.01	1.166	-0.739
5652.318	26.00	4.260	-1.949	6737.987	26.00	4.559	-1.749				

**Appendix**

**Table A2.** Elemental abundances from individual ions,  $\sigma$  is internal errors

HD 12484																	HD 13908																	HD 16175																	HD 17674																
Ion	[M/H]	$\sigma$	N	(M/H)	[M/H]	$\sigma$	N	(M/H)	[M/H]	$\sigma$	N	(M/H)	[M/H]	$\sigma$	N	(M/H)	[M/H]	$\sigma$	N	(M/H)	[M/H]	$\sigma$	N	(M/H)	[M/H]	$\sigma$	N	(M/H)																																							
Li I	–	–	1	2.85	–	–	1	1.38	–	–	1	3.00	–	–	1	1.80																																																			
C I	0.05	0.10	3	8.48	–0.08	0.08	3	8.35	0.29	0.10	3	8.72	–0.11	0.06	3	8.32																																																			
O I	0.09	–	1	8.78	0.01	–	1	8.70	0.40	–	1	9.09	0.01	–	1	8.70																																																			
Na I	0.01	0.12	3	6.25	0.00	0.10	3	6.24	0.43	0.03	2	6.75	–0.19	0.10	3	6.05																																																			
Mg I	0.07	0.12	4	7.67	–0.06	0.04	6	7.54	0.28	0.15	4	7.88	–0.11	0.08	4	7.49																																																			
Al I	0.03	0.06	2	6.48	–0.20	0.07	2	6.25	0.18	0.13	2	6.63	–0.30	0.06	2	6.15																																																			
Si I	0.12	0.12	13	7.63	0.10	0.07	12	7.61	0.34	0.13	10	7.85	–0.07	0.09	10	7.44																																																			
S I	–	–	–	–	–0.02	0.02	2	7.10	0.33	0.18	2	7.54	–0.16	–	1	6.96																																																			
Ca I	0.15	0.12	9	6.49	0.09	0.11	12	6.43	0.24	0.03	5	6.64	–0.14	0.16	9	6.2																																																			
Sc II	0.13	0.13	5	3.28	0.15	0.13	7	3.30	0.43	0.09	5	3.68	–0.03	0.10	6	3.12																																																			
Ti I	0.07	0.13	21	5.02	–0.06	0.09	24	4.89	0.39	0.06	16	5.34	–0.13	0.10	20	4.82																																																			
Ti II	0.02	0.11	3	4.97	0.00	0.08	5	4.95	0.38	0.18	4	5.32	–0.11	0.19	5	4.84																																																			
V I	0.01	0.05	7	3.94	–0.06	0.10	10	3.87	0.34	0.20	6	4.45	–0.14	0.12	6	3.79																																																			
Cr I	–0.01	0.12	19	5.63	–0.08	0.08	22	5.56	0.18	0.07	13	5.94	–0.22	0.09	21	5.42																																																			
Mn I	–0.15	0.13	5	5.28	–0.18	0.10	5	5.25	0.52	0.01	3	5.95	–0.07	0.11	5	5.36																																																			
Fe I	0.05	0.12	196	7.55	0.05	0.10	228	7.55	0.36	0.08	188	7.89	–0.14	0.11	215	7.36																																																			
Fe II	0.05	0.12	20	7.55	0.06	0.08	29	7.56	0.36	0.06	21	7.89	–0.15	0.10	25	7.35																																																			
Ni I	0.04	0.11	40	6.26	–0.03	0.10	50	6.19	0.33	0.06	39	6.65	–0.15	0.09	43	6.07																																																			
Zn I	0.04	0.06	3	4.60	0.08	0.02	4	4.64	0.37	–	1	4.88	–0.17	0.05	4	4.39																																																			
Y II	0.01	0.09	4	2.25	0.01	0.10	4	2.22	0.45	0.33	5	2.69	–0.17	0.14	5	2.07																																																			
Zr II	0.05	–	1	2.63	0.14	0.08	3	2.72	–	–	–	–	–0.02	0.10	3	2.56																																																			
Ba II	0.26	0.06	3	2.44	0.26	0.09	3	2.44	0.56	0.03	3	2.74	–0.04	0.07	3	2.14																																																			
Ce II	0.21	0.13	4	1.79	0.02	0.06	6	1.60	0.17	0.09	4	1.88	–0.15	0.13	6	1.43																																																			
Pr II	0.20	0.02	2	0.92	–0.11	0.05	4	0.61	0.18	0.24	4	0.99	–0.20	0.16	4	0.52																																																			
Nd II	0.05	0.13	2	1.47	–0.05	0.11	6	1.37	0.18	0.05	3	1.70	–0.11	0.12	6	1.31																																																			
Sm II	0.22	0.03	2	1.18	0.06	0.12	4	1.02	–	–	–	–	–0.01	0.14	2	0.95																																																			
Eu II	0.18	0.07	2	0.70	0.01	0.11	2	0.53	0.51	0.20	2	1.03	–0.03	0.06	2	0.49																																																			
HD 24040																	HD 29021																	HD 35759																	HD 89307																
Ion	[M/H]	$\sigma$	N	(M/H)	[M/H]	$\sigma$	N	(M/H)	[M/H]	$\sigma$	N	(M/H)	[M/H]	$\sigma$	N	(M/H)	[M/H]	$\sigma$	N	(M/H)	[M/H]	$\sigma$	N	(M/H)	[M/H]	$\sigma$	N	(M/H)																																							
Li I	–	–	1	1.10	–	–	1	1.00	–	–	1	2.73	–	–	1	2.25																																																			
C I	0.13	0.09	3	8.56	–0.18	0.08	3	8.25	0.04	0.09	3	8.47	–0.16	0.08	3	8.27																																																			
O I	0.14	–	1	8.83	–0.12	–	1	8.48	0.16	–	1	8.85	0.08	–	1	8.77																																																			
Na I	0.25	0.08	3	6.49	–0.21	0.09	3	6.03	–0.08	0.02	2	6.24	–0.09	0.04	3	6.15																																																			
Mg I	0.27	0.15	5	7.87	0.00	0.06	4	7.60	0.10	0.10	5	7.70	–0.04	0.11	5	7.56																																																			
Al I	0.17	0.05	2	6.62	–	–	–	–	–0.07	0.01	2	6.23	–0.19	0.04	2	6.26																																																			
Si I	0.27	0.11	15	7.78	–0.06	0.12	11	7.46	0.02	0.14	13	7.49	0.01	0.07	11	7.52																																																			
S I	0.16	0.03	2	7.28	–0.24	–	1	6.88	–0.11	0.11	2	7.10	–0.23	0.01	2	6.89																																																			
Ca I	0.24	0.10	10	6.58	–0.21	0.07	9	6.13	–0.03	0.08	8	6.35	–0.04	0.05	9	6.30																																																			
Sc II	0.29	0.05	6	3.44	–0.08	0.13	7	3.07	0.13	0.12	6	3.38	0.09	0.06	7	3.24																																																			
Ti I	0.28	0.08	23	5.23	–0.19	0.10	23	4.76	–0.08	0.07	19	4.95	0.01	0.07	25	4.96																																																			
Ti II	0.24	0.10	5	5.19	–0.21	0.16	4	4.74	–0.04	0.13	4	4.99	0.01	0.13	5	4.96																																																			
V I	0.27	0.04	9	4.20	–0.15	0.07	5	3.78	–0.21	0.07	6	3.90	–0.10	0.07	10	3.83																																																			
Cr I	0.16	0.06	22	5.80	–0.24	0.12	12	5.40	–0.21	0.09	19	5.55	–0.13	0.08	23	5.51																																																			
Mn I	0.21	0.06	5	5.64	–0.30	0.12	5	5.13	–0.18	0.10	5	5.25	–0.23	0.07	8	5.20																																																			
Fe I	0.23	0.10	220	7.73	–0.19	0.11	227	7.31	–0.04	0.08	192	7.54	–0.05	0.10	227	7.45																																																			
Fe II	0.22	0.09	29	7.72	–0.22	0.12	23	7.28	–0.04	0.06	19	7.54	–0.05	0.10	29	7.45																																																			
Ni I	0.31	0.05	48	6.53	–0.18	0.11	48	6.04	–0.05	0.07	40	6.25	–0.05	0.07	52	6.17																																																			
Zn I	0.33	0.12	4	4.89	–0.10	0.09	4	4.46	0.18	0.06	4	4.63	–0.07	0.11	4	4.49																																																			
Y II	0.15	0.17	4	2.36	–0.23	0.12	4	2.01	0.03	0.05	4	2.22	–0.12	0.12	5	2.09																																																			
Zr II	0.17	0.12	3	2.75	–0.17	0.09	3	2.41	0.09	0.19	2	2.67	–0.10	0.09	3	2.68																																																			
Ba II	0.14	0.06	3	2.32	–0.16	0.12	3	2.02	0.25	0.07	3	2.43	0.04	0.10	4	2.22																																																			
Ce II	0.10	0.11	6	1.68	–0.09	0.10	7	1.49	0.01	0.08	7	1.72	0.02	0.10	7	1.60																																																			
Pr II	0.05	0.14	4	0.77	–0.06	0.18	3	0.66	0.04	0.04	2	0.85	–0.10	0.11	4	0.62																																																			
Nd II	0.03	0.12	6	1.45	–0.05	0.12	7	1.37	–0.07	0.02	3	1.45	–0.01	0.06	6	1.41																																																			
Sm II	0.16	0.13	5	1.12	–	–	–	–	0.04	0.08	3	1.14	0.02	0.11	4	0.98																																																			
Eu II	0.06	0.11	2	0.58	–0.07	0.03	2	0.45	0.03	0.14	2	0.55	0.13	0.11	2	0.58																																																			

N – is the number of lines used in analysis

Table A2 (continued)

Table A2 (continued)																
HD 113337				HD 141399				HD 143105				HD 150706				
Ion	[M/H]	$\sigma$	N	(M/H)	[M/H]	$\sigma$	N	(M/H)	[M/H]	$\sigma$	N	(M/H)	[M/H]	$\sigma$	N	(M/H)
Li I	–	–	1	–	–	–	1	0.71	–	–	1	2.30	–	–	1	2.60
C I	0.06	0.05	3	8.49	0.14	0.07	3	8.70	0.10	0.09	3	8.53	–0.13	0.09	3	8.30
O I	0.11	–	1	8.8	0.41	–	1	9.10	0.09	–	1	8.78	0.07	–	1	8.76
Na I	0.09	0.06	3	6.33	0.36	0.04	2	6.68	0.07	0.13	3	6.31	–0.11	0.06	3	6.13
Mg I	0.12	0.08	6	7.72	0.41	0.1	4	8.01	0.11	0.10	5	7.71	–0.03	0.07	6	7.57
Al I	0.01	0.06	2	6.46	0.40	0.08	2	6.70	–0.01	0.06	2	6.43	–0.16	0.07	2	6.29
Si I	0.21	0.03	9	7.72	0.43	0.15	10	7.94	0.10	0.04	12	7.61	0.08	0.06	12	7.59
S I	0.09	0.04	2	7.21	0.22	–	1	7.43	–0.02	0.08	2	7.10	–0.12	0.08	2	7.00
Ca I	0.17	0.06	10	6.51	0.38	0.06	6	6.72	0.07	0.11	10	6.41	0.08	0.10	10	6.42
Sc II	0.15	0.10	7	3.3	0.59	0.13	6	3.84	0.02	0.09	7	3.17	0.14	0.08	7	3.29
Ti I	0.07	0.05	24	5.02	0.45	0.06	17	5.40	–0.10	0.12	25	4.85	0.04	0.08	25	4.99
Ti II	0.08	0.07	5	5.03	0.45	0.18	4	5.40	–0.10	0.15	4	4.85	0.06	0.13	5	5.01
V I	0.06	0.08	9	3.99	0.34	0.09	7	4.45	–0.03	0.11	10	3.90	–0.07	0.06	11	3.86
Cr I	0.14	0.04	23	5.78	0.24	0.08	17	6.00	–0.13	0.10	23	5.51	–0.03	0.07	23	5.61
Mn I	–0.05	0.09	8	5.38	0.49	0.15	4	5.92	–0.05	0.10	7	5.38	–0.08	0.1	5	5.35
Fe I	0.14	0.09	229	7.64	0.47	0.10	190	7.97	0.01	0.11	216	7.51	0.05	0.11	222	7.55
Fe II	0.15	0.09	31	7.65	0.47	0.08	21	7.97	0.00	0.11	31	7.50	0.04	0.09	29	7.54
Ni I	0.09	0.10	50	6.31	0.40	0.07	39	6.70	–0.05	0.10	50	6.17	0.01	0.08	49	6.23
Zn I	0.09	0.06	4	4.65	0.55	0.04	2	4.99	0.01	0.06	4	4.57	0.06	0.04	4	4.62
Y II	0.06	0.09	6	2.27	0.38	0.06	2	2.57	–0.03	0.11	6	2.18	0.01	0.09	5	2.22
Zr II	0.12	0.07	3	2.70	0.37	0.10	3	3.25	–0.02	0.14	3	2.56	0.13	0.12	3	2.71
Ba II	0.33	0.08	3	2.51	0.52	0.07	3	2.70	0.05	0.02	3	2.23	0.36	0.06	3	2.54
Ce II	0.06	0.10	7	1.64	0.48	0.10	5	2.19	0.04	0.12	6	1.62	0.06	0.13	7	1.64
Pr II	–0.03	0.07	4	0.69	0.36	0.22	4	1.17	–0.03	0.12	5	0.69	–0.07	0.09	4	0.65
Nd II	0.02	0.10	7	1.44	0.42	0.07	5	1.94	–0.02	0.14	6	1.4	0.13	0.10	9	1.55
Sm II	0.04	0.03	4	1.00	–	–	–	–	0.08	0.12	3	1.04	0.02	0.13	3	0.98
Eu II	0.15	0.06	2	0.67	0.32	0.19	2	0.84	0.04	0.10	2	0.56	0.05	0.11	2	0.53
HD 154345				HD 159243				HD 164595				HD 191806				
Ion	[M/H]	$\sigma$	N	(M/H)	[M/H]	$\sigma$	N	(M/H)	[M/H]	$\sigma$	N	(M/H)	[M/H]	$\sigma$	N	(M/H)
Li I	–	–	1	0.5	–	–	1	2.6	–	–	1	1.00	–	–	1	2.81
C I	–0.18	0.13	3	8.25	0.04	0.07	3	8.47	–0.07	0.06	3	8.36	0.25	0.04	3	8.68
O I	–0.04	–	1	8.65	0.06	–	1	8.75	–0.05	–	1	8.64	0.28	–	1	8.97
Na I	–0.04	0.07	3	6.20	–0.01	0.02	2	6.31	–0.06	0.09	3	6.18	0.34	0.03	2	6.66
Mg I	–0.03	0.07	6	7.57	0.02	0.11	2	7.62	0	0.06	6	7.60	0.25	0.09	3	7.85
Al I	–0.14	0.06	2	6.31	–0.17	0.04	2	6.28	–0.12	0.05	2	6.33	0.26	0.01	2	6.56
Si I	–0.01	0.12	15	7.50	0.07	0.12	11	7.58	0.01	0.07	11	7.52	0.28	0.13	9	7.79
S I	–0.13	0.07	2	6.99	–0.06	–	1	7.15	–0.05	0.07	2	7.07	0.19	–	1	7.40
Ca I	–0.07	0.08	10	6.27	–0.02	0.04	6	6.36	–0.03	0.06	10	6.31	0.22	0.06	3	6.60
Sc II	0.03	0.07	6	3.18	0.21	0.15	6	3.46	0.07	0.08	7	3.22	0.35	0.08	4	3.60
Ti I	–0.01	0.09	27	4.94	0.08	0.09	15	5.03	0.03	0.05	24	4.98	0.28	0.08	18	5.23
Ti II	–0.12	0.12	4	4.83	0.04	0.14	4	4.99	0.00	0.13	5	4.95	0.27	0.12	4	5.22
V I	0.02	0.08	10	3.95	–0.19	0.01	4	3.92	0.01	0.07	10	3.94	0.11	0.06	6	4.22
Cr I	–0.1	0.07	22	5.54	–0.13	0.1	16	5.63	–0.06	0.08	23	5.58	0.18	0.07	16	5.94
Mn I	0.17	0.13	5	5.60	0.13	0.06	5	5.64	–0.03	0.06	5	5.46	0.32	0.11	4	5.75
Fe I	–0.05	0.10	229	7.45	0.14	0.08	193	7.64	–0.01	0.11	229	7.49	0.36	0.09	195	7.86
Fe II	–0.03	0.10	33	7.47	0.15	0.04	21	7.65	–0.02	0.09	31	7.48	0.38	0.05	22	7.88
Ni I	–0.04	0.06	48	6.18	–0.01	0.06	36	6.29	0.02	0.08	51	6.24	0.32	0.05	40	6.62
Zn I	–0.05	0.11	4	4.51	0.23	0.12	4	4.68	–0.01	0.04	4	4.55	0.49	0.03	2	4.94
Y II	–0.03	0.13	6	2.18	0.32	0.04	3	2.51	–0.06	0.09	5	2.15	0.34	0.20	4	2.58
Zr II	0.1	0.09	3	2.68	0.11	0.08	2	2.79	0.04	0.12	3	2.62	0.42	0.11	3	3.00
Ba II	0.01	0.03	2	2.19	0.32	0.08	3	2.50	0.08	0.05	3	2.26	0.42	0.12	3	2.60
Ce II	0.02	0.08	10	1.60	0.16	0.11	4	1.88	0.01	0.10	9	1.59	0.42	0.15	4	2.00
Pr II	–0.06	0.14	4	0.66	0.22	0.17	3	1.03	–0.12	0.13	4	0.59	0.32	0.16	3	1.04
Nd II	0.05	0.11	9	1.47	0.24	0.09	3	1.76	–0.02	0.06	8	1.40	0.34	0.15	4	1.76
Sm II	0.10	0.13	5	1.06	0.20	0.06	2	1.30	0.00	0.11	4	0.96	0.43	–	1	1.39
Eu II	0.10	0.11	2	0.62	0.16	0.18	2	0.68	0.03	0.14	2	0.55	0.23	0.14	2	0.75

N – is the number of lines used in analysis



Table A2 (continued)

Table A2 (continued)																
HD 214823				HD 219828				HD 220842				HD 221585				
Ion	[M/H]	$\sigma$	N	(M/H)	[M/H]	$\sigma$	N	(M/H)	[M/H]	$\sigma$	N	(M/H)	[M/H]	$\sigma$	N	(M/H)
Li I	–	–	1	1.50	–	–	–	2.30	–	–	1	1.16	–	–	–	1.62
C I	0.06	0.10	3	8.49	0.11	0.06	3	8.54	–0.13	0.05	3	8.30	0.29	0.06	3	8.72
O I	0.11	–	1	8.80	0.13	–	1	8.82	–0.06	–	1	8.63	0.28	–	1	8.97
Na I	0.16	0.02	3	6.40	0.13	0.15	3	6.37	–0.16	0.02	3	6.08	0.30	0.15	3	6.54
Mg I	0.15	0.06	6	7.75	0.16	0.05	4	7.76	–0.07	0.09	6	7.53	0.30	0.15	4	7.90
Al I	0.04	0.11	2	6.49	0.08	0.08	2	6.53	–0.28	0.01	2	6.17	0.24	0.05	2	6.69
Si I	0.16	0.09	14	7.67	0.33	0.09	13	7.84	–0.09	0.08	12	7.42	0.27	0.12	12	7.78
S I	0.16	0.08	3	7.28	0.14	0.05	2	7.26	–0.14	0.03	2	6.98	0.28	–	1	7.40
Ca I	0.12	0.07	10	6.46	0.16	0.13	9	6.50	–0.11	0.10	12	6.23	0.18	0.09	8	6.52
Sc II	0.12	0.09	6	3.27	0.32	0.07	7	3.47	–0.01	0.12	7	3.14	–	–	–	–
Ti I	0.13	0.09	25	5.08	0.22	0.11	23	5.17	–0.14	0.09	27	4.81	0.34	0.11	26	5.29
Ti II	0.10	0.09	4	5.05	0.18	0.23	5	5.13	–0.16	0.12	5	4.79	0.30	0.03	3	5.25
V I	0.10	0.11	12	4.03	0.22	0.16	6	4.15	–0.16	0.11	11	3.77	0.40	0.12	8	4.33
Cr I	0.07	0.10	23	5.71	0.09	0.11	23	5.73	–0.18	0.08	23	5.46	0.24	0.12	19	5.88
Mn I	0.07	0.05	5	5.50	0.04	0.09	5	5.47	–0.13	0.02	5	5.30	0.25	0.12	4	5.68
Fe I	0.13	0.11	224	7.63	0.19	0.12	202	7.69	–0.1	0.11	224	7.40	0.33	0.13	210	7.83
Fe II	0.10	0.11	31	7.60	0.16	0.13	21	7.66	–0.11	0.09	31	7.39	0.32	0.12	25	7.82
Ni I	0.14	0.07	47	6.36	0.25	0.11	42	6.47	–0.14	0.08	52	6.08	0.41	0.11	48	6.63
Zn I	0.14	0.08	4	4.70	0.14	0.04	4	4.70	–0.04	0.12	4	4.52	0.36	0.11	4	4.92
Y II	0.05	0.10	6	2.26	0.08	0.09	4	2.32	0.03	0.15	5	2.24	0.46	0.20	3	2.70
Zr II	0.10	0.11	3	2.68	0.24	0.10	3	2.82	0.05	0.08	3	2.63	0.42	0.05	3	3.00
Ba II	0.21	0.05	3	2.39	0.04	0.06	3	2.22	0.09	0.08	3	2.27	0.25	0.09	3	2.43
Ce II	–0.01	0.06	9	1.57	0.12	0.08	7	1.70	0.04	0.06	10	1.62	0.26	0.10	7	1.84
Pr II	–0.14	0.06	4	0.58	0.03	0.1	3	0.75	–0.09	0.07	4	0.63	0.17	0.15	3	0.89
Nd II	0.01	0.05	10	1.43	0.18	0.14	6	1.60	0	0.13	9	1.42	0.35	0.15	6	1.77
Sm II	0.06	0.12	5	1.02	0.19	0.14	4	1.15	0.18	0.17	6	1.14	–	–	–	–
Eu II	0.15	0.12	2	0.67	0.16	0.16	2	0.68	0.05	0.18	2	0.57	0.16	0.14	2	0.68
HD 222155				HIP 65407				HIP 91258				HIP 109384				
Ion	[M/H]	$\sigma$	N	(M/H)	[M/H]	$\sigma$	N	(M/H)	[M/H]	$\sigma$	N	(M/H)	[M/H]	$\sigma$	N	(M/H)
Li I	–	–	1	0.93	–	–	1	1.09	–	–	1	0.0	–	–	1	0.5
C I	–0.11	0.09	3	8.32	0.27	0.10	3	8.70	0.27	0.09	3	8.70	–0.13	0.06	3	8.30
O I	0.07	–	1	8.76	0.36	–	1	9.05	0.40	–	1	9.00	0.00	0.06	1	8.69
Na I	–0.11	0.05	3	6.13	0.34	0.04	2	6.66	0.32	–	3	6.56	–0.25	0.16	3	5.99
Mg I	–0.01	0.11	3	7.59	0.28	0.06	3	7.88	0.30	0.04	3	7.90	0.01	0.12	3	7.60
Al I	–0.12	0.07	2	6.33	0.26	0.03	2	6.56	0.2	0.06	2	6.51	–0.17	0.02	2	6.28
Si I	–0.02	0.12	14	7.49	0.26	0.18	12	7.77	0.25	0.19	12	7.76	–0.07	0.12	10	7.44
S I	–0.08	0.12	3	7.04	0.02	–	1	7.23	–0.08	–	1	7.13	–0.23	–	1	6.89
Ca I	–0.04	0.11	11	6.30	0.21	0.08	6	6.59	0.27	0.09	3	6.61	–0.26	0.11	8	6.08
Sc II	0.08	0.06	6	3.23	0.40	0.10	5	3.65	0.49	0.12	6	3.64	–0.06	0.11	5	3.09
Ti I	–0.05	0.09	27	4.90	0.28	0.11	20	5.23	0.29	0.07	18	5.24	–0.16	0.13	19	4.79
Ti II	–0.05	0.10	5	4.90	0.25	0.19	3	5.20	0.19	0.16	3	5.14	–0.17	0.19	4	4.78
V I	–0.14	0.07	9	3.79	0.37	0.13	7	4.48	0.48	0.21	7	4.41	–0.09	0.10	5	3.84
Cr I	–0.15	0.09	23	5.49	0.19	0.11	18	5.95	0.25	0.07	14	5.89	–0.35	0.13	22	5.29
Mn I	–0.09	0.10	5	5.34	0.29	0.05	4	5.75	0.23	0.10	4	5.66	–0.43	0.11	5	5.00
Fe I	–0.06	0.09	222	7.44	0.35	0.09	188	7.85	0.30	0.10	178	7.80	–0.24	0.13	196	7.26
Fe II	–0.05	0.08	31	7.45	0.33	0.09	19	7.83	0.27	0.12	15	7.77	–0.26	0.08	19	7.24
Ni I	–0.07	0.07	49	6.15	0.35	0.10	42	6.65	0.25	0.09	36	6.55	–0.16	0.11	44	6.06
Zn I	0.02	0.03	4	4.58	0.49	0.11	3	4.94	–	–	–	–	–0.13	0.06	3	4.43
Y II	0.06	0.11	5	2.27	0.59	0.24	4	2.78	–	–	–	–	–0.23	0.18	4	2.01
Zr II	0.09	0.11	3	2.67	0.54	0.18	3	3.12	0.63	–	2	3.21	0.08	0.14	3	2.66
Ba II	0.19	0.08	3	2.37	0.40	0.04	3	2.58	0.37	–	1	2.55	–0.23	0.11	3	1.95
Ce II	0.07	0.10	10	1.65	0.44	0.13	5	2.15	0.52	–	1	2.10	–0.19	0.04	3	1.39
Pr II	–0.20	0.03	4	0.52	0.52	0.21	4	1.33	0.25	–	1	0.97	–0.1	0.08	2	0.62
Nd II	0.11	0.09	9	1.53	0.23	0.12	3	1.75	0.47	0.20	3	1.89	–0.06	0.18	4	1.36
Sm II	0.04	0.16	5	1.00	0.51	0.38	3	1.61	–	–	–	–	–	–	–	–
Eu II	0.13	0.14	2	0.52	0.30	0.14	2	0.62	0.28	0.14	2	0.80	–0.07	–	1	0.45

N – is the number of lines used in analysis

**Table A2 (continued)**

HIP 109600				
Ion	[M/H]	$\sigma$	N	(M/H)
Li I	–	–	1	1.00
C I	–0.02	0.04	2	8.41
O I	–0.06	–	1	8.63
Na I	–0.13	0.01	2	6.19
Mg I	0.11	0.07	3	7.70
Al I	–0.01	0.01	2	6.29
Si I	–0.08	0.12	11	7.43
S I	–	–	–	–
Ca I	–0.15	0.10	2	6.23
Sc II	0.1	0.12	6	3.35
Ti I	0.04	0.07	20	4.99
Ti II	0.02	0.22	3	4.97
V I	–0.09	0.14	6	4.02
Cr I	–0.26	0.10	16	5.50
Mn I	–0.18	0.06	3	5.25
Fe I	–0.07	0.10	183	7.43
Fe II	–0.08	0.09	21	7.42
Ni I	–0.13	0.06	38	6.17
Zn I	0.09	–	1	4.54
Y II	0.16	0.13	3	2.41
Zr II	0.02	0.20	2	2.90
Ba II	–0.02	0.13	2	2.16
Ce II	0.03	0.12	3	1.74
Pr II	–0.09	0.13	2	0.63
Nd II	0.04	0.05	3	1.56
Sm II	–	–	–	–
Eu II	0.18	–	1	0.70

N – is the number of the lines used in analysis.

